

# An X-Ray and Electron Paramagnetic Resonance Structural Investigation of Oxygen Discrimination during the Collapse of Methyl-Benzoyloxy Radical Pairs in Crystalline Acetyl Benzoyl Peroxide<sup>1a,b</sup>

Nathan J. Karch,<sup>1c</sup> Edward T. Koh, Bonnie L. Whitsel, and J. Michael McBride\*<sup>1d</sup>

Contribution from the Department of Chemistry, Yale University, New Haven, Connecticut 06520. Received October 25, 1974

**Abstract:** Partial photolysis of crystalline acetyl benzoyl peroxide (ABP) at low temperature yields methyl benzoate and toluene. Isotope labeling shows that these are cage products and that the oxygen atoms of benzoyloxy do not scramble completely in ester formation. Since carboxy inversion is not important, the ester probably derives from methyl-benzoyloxy radical pairs (M-B), some of which can be observed by low-temperature EPR. The crystal structure of ABP, determined by low-temperature X-ray diffraction ( $P2_1/c$ ), and the  $g$  and  $D$  tensors of M-B are reported. Substantial motion of the methyl radical during formation of M-B is inferred by analysis of the  $D$  tensor. Oxygen discrimination in ester formation is rationalized in terms of M-B geometry and the position, determined by packing analysis, of the accompanying  $\text{CO}_2$  molecule. A  ${}^2A_2$   $\pi$  ground state of  $C_{2v}$  symmetry is tentatively assigned to the benzoyloxy radical on the basis of INDO calculations together with EPR and  ${}^{13}\text{C}$  CIDNP evidence. An iterative method allows least-squares refinement of triplet state  $D$  and  $g$  tensors from EPR data collected on crystals in general orientations.

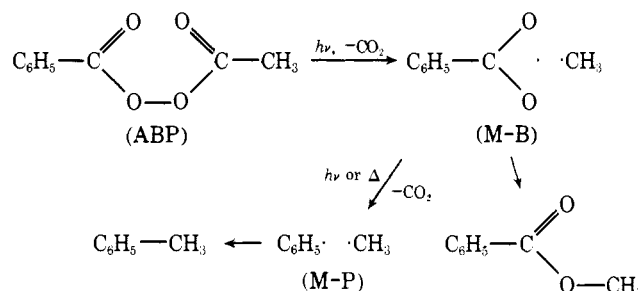
In recent years there has been increasing interest in the thermal and photochemical reactions of organic solids.<sup>2</sup> In addition to the technological and biochemical relevance of such reactions, this interest has been motivated by the potential for synthetic chemistry of reactions in the regular, rigid molecular environment of an organic crystal. Solid-state reactions hold equal promise for mechanistic chemistry since they provide a unique perspective on solution processes as well as posing their own new problems.

Many of the tools developed for studying the mechanism of solution reactions are not appropriate for studying reactions in crystals. For example, studies of concentration dependence or of modest perturbations from unreactive substituents are rarely possible for crystal reactions. At the same time there are other techniques uniquely suited to studying the reactions of solids. The purpose of our work with acetyl benzoyl peroxide (ABP) is to show how single-crystal EPR spectroscopy and X-ray diffraction can be used to elucidate the mechanism of solid-state radical-pair reactions.<sup>3</sup> The power of these methods is such that this class of reactions may be among the most fruitful for demonstrating the general mechanistic features of organic solid-state chemistry.

This paper concentrates on structural aspects of the formation of methyl benzoate during photolysis of crystalline ABP. In a subsequent paper we will discuss the thermal and photochemical dynamics of this system.<sup>4</sup>

## Results and Discussion

ABP melts at 38°C. Thermolysis or photolysis of the pure liquid at higher temperature leads to a host of aromatic products.<sup>5</sup> Among these, the products of induced decomposition predominate at low conversion.<sup>5</sup> We find that photolysis of the pure, crystalline solid at temperatures from 65 K to 20°C and to conversions of 0.016 to 35% gives methyl benzoate and toluene.<sup>6</sup> The ratio of methyl benzoate to toluene varies in a complex way from 1:3 to 3:1 with changes in temperature, conversion, and irradiating wavelength.<sup>4</sup> No other products can be observed in the  ${}^1\text{H}$  NMR spectrum of the crude photolysis mixture although, after photolysis to low conversion at -70°C, the product mixture contained 1.5% methane and 0.7% ethane by mass spectrometry.



**Cage Effect.** The possibility that the solid-state photolysis products might arise by an intermolecular induced decomposition path was tested in crossover experiments. Mixed crystals were prepared by removing ether from a nearly equimolar solution of normal and perdeuterated ABP which had been stirred for 16 hr. Mass spectral analysis after photolysis to 15% conversion at -65 to -70°C showed that less than 0.5% of the methyl benzoate and about 1.4% of the toluene contained both protium and deuterium ( $d_3$  and  $d_5$ ). Thus less than 1% of the ester and less than 3% of the toluene had formed intermolecularly.<sup>7</sup>

Using a combination of isotope dilution and EPR spin-counting techniques, we have shown that, at least at low temperature and low conversion, toluene is formed by collapse of a geminate methyl-phenyl radical pair (M-P).<sup>4</sup> A similar proof is lacking for the ester, and it is well known that thermolysis of some diacyl peroxides leads to ester products through alkylacyl carbonates, which form in an ionic carboxy inversion process.<sup>9</sup> This complication has not arisen in photolysis experiments,<sup>10</sup> and we find that authentic methylbenzoyl carbonate is stable to our photolysis conditions. Although we cannot be certain that the carbonate would be photostable if formed within an ABP crystal, we assume that methyl benzoate is formed by cage coupling of methyl-benzoyloxy radical pairs (M-B).

**Oxygen Discrimination.** In a fluid medium, very little motion is required for the oxygen atoms of the M-B radical pair to become statistically equivalent. In a rigid medium with low site symmetry, the smallest motion which can lead to statistical equivalence of the oxygens is rotation of the carboxyl group about the phenyl-carboxyl bond. Since collapse of the M-B pair may be faster than the scrambling

Table I. Atomic Fractional Coordinates

Atom	x	y	z
C(1) <sup>a</sup>	-0.44512 (26)	0.04363 (32)	-0.14136 (17)
C(2)	-0.32758 (19)	0.00978 (23)	-0.21011 (13)
C(3)	-0.10172 (20)	0.18946 (22)	-0.33006 (11)
C(4)	0.03570 (18)	0.17014 (20)	-0.38555 (11)
C(5)	0.17249 (19)	0.07425 (22)	-0.35184 (12)
C(6)	0.29633 (20)	0.06161 (23)	-0.40696 (13)
C(7)	0.28482 (21)	0.14356 (25)	-0.49528 (13)
C(8)	0.14950 (22)	0.23861 (26)	-0.52933 (13)
C(9)	0.02533 (20)	0.25260 (24)	-0.47430 (13)
O(1)	-0.33782 (14)	-0.09002 (16)	-0.27636 (9)
O(2)	-0.19817 (13)	0.11922 (16)	-0.18592 (8)
O(4)	-0.21963 (14)	0.27648 (17)	-0.34977 (9)
O(3)	-0.07490 (13)	0.08814 (17)	-0.24725 (8)
H(1)	-0.519 (3)	0.142 (3)	-0.170 (2)
H(2)	-0.396 (2)	0.080 (3)	-0.081 (2)
H(3)	-0.510 (3)	-0.057 (3)	-0.136 (2)
H(5) <sup>b</sup>	0.181	0.016	-0.288
H(6)	0.393	-0.006	-0.382
H(7)	0.373	0.132	-0.533
H(8)	0.141	0.296	-0.592
H(9)	-0.070	0.320	-0.498
C'(1) <sup>c</sup>	-0.370	-0.103	0.006
C'(2) <sup>d</sup>	-0.467	-0.007	-0.188
O'(1) <sup>d</sup>	-0.354	-0.061	-0.275
O'(2) <sup>d</sup>	-0.580	0.048	-0.102

<sup>a</sup>Coordinates for C(1) through H(3) were refined by least-squares using the X-ray data. Estimated standard deviation in the last digit is given in parentheses. <sup>b</sup>H(5) through H(9) are aryl hydrogens. Their positions were assumed to be 0.98 Å from C(5) through C(9), respectively, in the appropriate direction. These were not varied in fitting the X-ray data. <sup>c</sup>Positioned to give the best least-squares fit to the experimental *D* tensor assuming that the atomic coordinates of the  $\pi$ -benzoyloxy radical match those in undamaged ABP and that the  $\pi$  spread is zero (see text). <sup>d</sup>Positioned by hard-sphere packing analysis assuming C'(1) has the position indicated and that all other atoms are positioned as in undamaged ABP. Nonbonded H-O, C-O, and O-O distances are greater than 2.5, 2.8, and 2.8 Å, respectively.

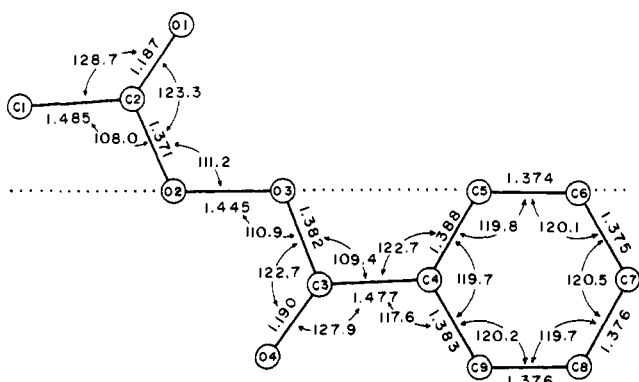


Figure 1. Bond lengths (Å) and angles for ABP.

process, it is not surprising to find that, in rigid media, the methyl radical can discriminate between the oxygens of the geminate benzoyloxy radical in ester formation.

When ABP with 98% <sup>18</sup>O in the peroxidic positions was photolyzed to completion in ethanol solvent at 0°C, the mass spectrum of methyl benzoate product showed equal abundances for the *m/e* 105 and 107 benzoyl cation fragments, implying complete scrambling of the benzoyloxy oxygens.<sup>11</sup> Since the oxygens of methyl benzoate do not scramble in the mass spectrometer,<sup>12</sup> they almost certainly scrambled in the M-B pair.<sup>13</sup>

When a similar experiment was conducted in glassy ethanol at 77 K, the benzoyl cation isotopic abundances showed only 55% scrambling, implying that methyl radicals couple with the former peroxy oxygen of geminate benzoyloxy rad-

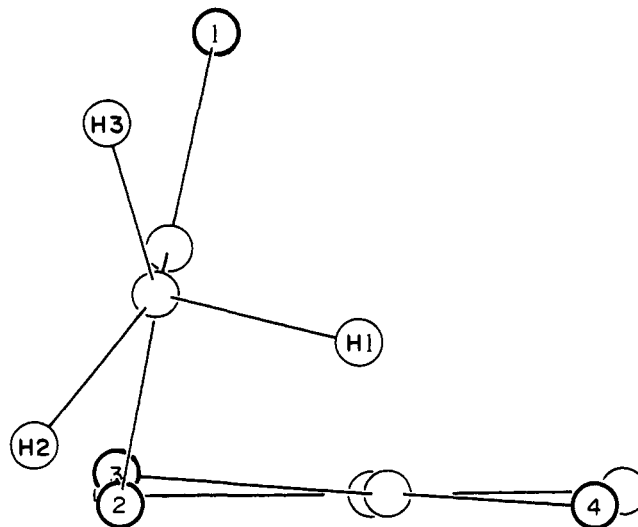


Figure 2. View of ABP along C(5)-C(6). Oxygens and methyl hydrogens are numbered, ring hydrogens omitted.

icals 2.6 to 2.7 times more often than with the former carbonyl oxygen.

Less dramatic discrimination was found after photolysis of crystalline ABP to 8% conversion at -70°C. Here the factor favoring coupling with the former peroxy oxygen was 1.65. The observed scrambling cannot be due to photoisomerization of ABP since a control experiment showed less than 0.3% scrambling after 3% decomposition at this temperature. Other work in our laboratory suggests that methyl benzoate is formed by at least two independent radical-pair pathways.<sup>4</sup> The remainder of this paper concentrates on the predominant pathway, which we believe leads to coupling through the former peroxy oxygen. We begin by discussing this discrimination in terms of the structure of crystalline ABP.

**Molecular Structure.** ABP crystallizes in space group *P*2<sub>1</sub>/*c* with four molecules in the unit cell. The asymmetric unit is thus a single molecule. The fractional atomic coordinates and thermal parameters of Tables I and II were determined by least-squares fitting to 1388 independent X-ray reflections measured diffractometrically at -95°C. Bond distances and angles among nonhydrogen atoms are shown in Figure 1. These are not corrected for thermal motion, which is modest and fairly isotropic at low temperature. Based on the variance-covariance matrix from least-squares refinement, the largest estimated standard deviation in a bond distance is 0.0026 Å and in a bond angle 0.18°. Hydrogen positions were refined only for the methyl group; the three carbon-hydrogen distances range from 0.93 to 1.02 Å and the six bond angles at C(1) from 106 to 112°.

All nonhydrogen atoms of the molecule lie within 0.04 Å of one of the two planes which would be formed by folding Figure 1 along the dotted line to a dihedral angle of 78.2°. A projection of the molecule along the C(5)-C(6) axis (Figure 2) shows the conformation. The acetoxy fragment, C(1)-C(2)-O(1)-O(2), and the carbon atoms of the benzoyloxy fragment, C(3) through C(9), are each planar within experimental error (largest deviation 0.003 Å). The O(3)-C(3)-O(4) carboxyl group is twisted by 4.6° relative to the phenyl plane. The acylperoxy groups O(1)-C(2)-O(2)-O(3) and O(4)-C(3)-O(3)-O(2) are not quite eclipsed, having torsional angles of 3.6 and 6.3°, respectively. The torsional angle of the peroxide bond, C(2)-O(2)-O(3)-C(3), is 86.6°. The estimated uncertainty in these torsional and dihedral angles is 0.2°. The torsional angle H(1)-C(1)-C(2)-O(2) is 90 ± 2°.

Table II. Thermal Parameters<sup>a</sup>

Atom	Anisotropic parameters $\times 10^4$						Principal rms vibrational amplitudes, Å		
	$\beta_{11}$	$\beta_{22}$	$\beta_{33}$	$\beta_{12}$	$\beta_{13}$	$\beta_{23}$			
C(1)	159 (3)	220 (5)	76 (2)	5 (4)	32 (2)	14 (2)	0.222 (3)	0.245 (3)	0.285 (3)
C(2)	136 (3)	165 (3)	56 (1)	13 (3)	5 (1)	17 (2)	0.198 (2)	0.295 (2)	0.198 (2)
C(3)	142 (3)	151 (3)	55 (1)	-15 (3)	9 (1)	-12 (2)	0.196 (2)	0.228 (2)	0.239 (2)
C(4)	127 (3)	132 (3)	51 (1)	-9 (2)	7 (1)	-10 (1)	0.187 (2)	0.214 (2)	0.228 (2)
C(5)	144 (3)	170 (3)	54 (1)	4 (3)	9 (1)	3 (2)	0.218 (2)	0.226 (2)	0.232 (2)
C(6)	131 (3)	204 (4)	68 (1)	14 (3)	10 (1)	-5 (2)	0.211 (2)	0.241 (2)	0.260 (2)
C(7)	148 (3)	231 (4)	62 (1)	-12 (3)	24 (2)	-15 (2)	0.217 (2)	0.237 (2)	0.271 (2)
C(8)	180 (3)	228 (5)	54 (1)	-12 (3)	12 (2)	11 (2)	0.224 (2)	0.247 (2)	0.265 (2)
C(9)	141 (3)	181 (4)	59 (1)	3 (3)	3 (2)	3 (2)	0.218 (2)	0.228 (2)	0.247 (2)
O(1)	208 (2)	197 (3)	67 (1)	-20 (2)	13 (1)	-13 (1)	0.226 (2)	0.262 (2)	0.275 (2)
O(2)	153 (2)	266 (3)	58 (1)	-39 (2)	29 (1)	-22 (1)	0.208 (2)	0.230 (2)	0.295 (2)
O(3)	135 (2)	277 (3)	55 (1)	5 (2)	18 (1)	11 (1)	0.212 (2)	0.234 (2)	0.283 (2)
O(4)	160 (2)	218 (3)	84 (1)	50 (2)	29 (1)	9 (1)	0.205 (2)	0.264 (2)	0.295 (2)

Atom	<i>B</i>	Amp <sup>b</sup>	Atom	<i>B</i>	Amp	Atom	<i>B</i>	Amp	Atom	<i>B</i>	Amp
H(1)	7.8 (6)	0.32	H(2)	8.0 (6)	0.32	H(3)	8.4 (6)	0.33	H(5)	5.2 (4)	0.26
H(6)	4.9 (4)	0.25	H(7)	6.0 (4)	0.28	H(8)	5.8 (4)	0.27	H(9)	5.1 (4)	0.25

<sup>a</sup> Estimated standard deviations in the final digit are given in parentheses. Anisotropic factors of the form  $\exp[-(h^2\beta_{11} + k^2\beta_{22} + l^2\beta_{33} + 2hk\beta_{12} + 2hl\beta_{13} + 2kl\beta_{23})]$ . <sup>b</sup> Isotropic rms vibrational amplitude (Å).

Table III. Intermolecular Distances Less Than 3.5 Å Among Nonhydrogen Atoms

Atoms		Distance, Å <sup>a</sup>	Key <sup>b</sup>
C(5)	O(1)	3.297 (2)	a
C(7)	O(1)	3.312 (3)	b
C(1)	O(1)	3.416 (3)	c
C(1)	O(4)	3.445 (3)	d
C(9)	O(2)	3.447 (2)	e
C(3)	O(3)	3.449 (2)	f
C(5)	O(2)	3.451 (3)	g
C(8)	O(1)	3.497 (2)	h

<sup>a</sup> Estimated standard deviation ( $\times 10^3$ ) in parentheses. <sup>b</sup> Identification in Figures 3 and 4.

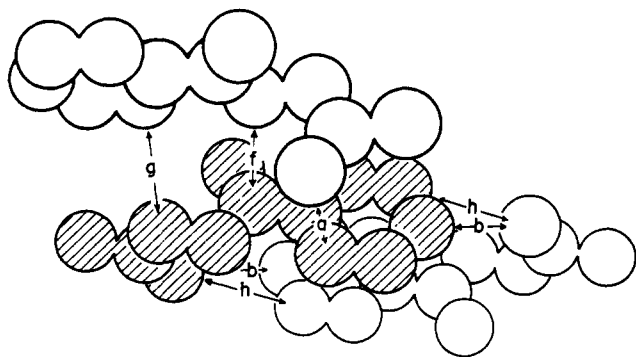


Figure 3. View showing out-of-plane neighbors of the benzoyloxy group of ABP (crystallographic *b* vertical). Hydrogens are omitted, and intermolecular distances less than 3.5 Å are coded by letters given in Table III. The implicit atomic radii are of no significance.

The observed molecular geometry is in accord with earlier, less precise diaryl peroxide structures based on photographic intensity data collected at ambient temperature.<sup>14</sup> It is particularly close to the structure of dibenzoyl peroxide, which has a C-O-O-C torsional angle of 91°. <sup>14a,15</sup>

**Crystal Packing.** There are no unusual intermolecular contacts. The six distances less than 3.5 Å which do not involve hydrogen are shown in Table III and illustrated in Figures 3, 4, and 5. The benzoyloxy portion of the shaded molecule in Figure 3 is sandwiched on the lower face by a benzoyloxy group across the center of symmetry at (0, 0, -1/2), and on the upper by the acetylperoxy fragment of a molecule related by the screw axis at  $a = 0, c = -1/4$ . The distance between the parallel phenyl planes is 3.555 Å. The phenyl plane makes a dihedral angle of 11.7° with the least-

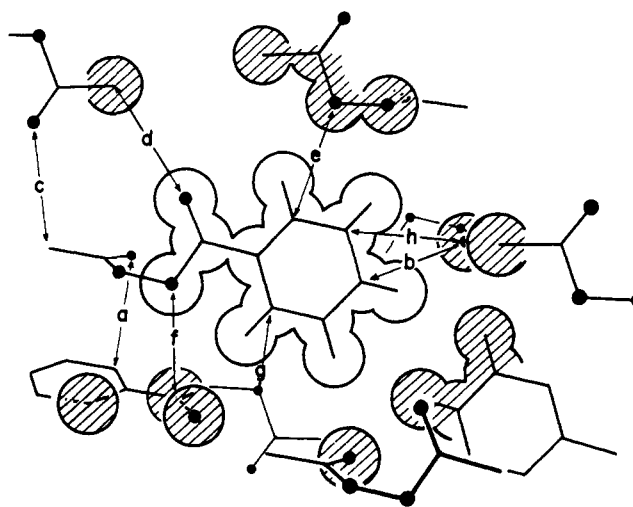


Figure 4. View normal to benzoyloxy group of ABP with the neighboring atoms nearly in its plane shaded. Methyl hydrogens are omitted; oxygens denoted by solid dots; implicit atomic radii are insignificant.

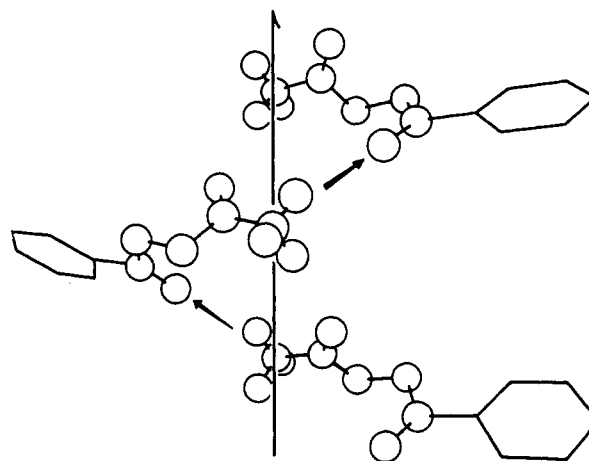


Figure 5. Molecules related by the screw axis (-0.25, *y*, -0.25) with ring hydrogens omitted. Arrows show the 3.45 Å C(1)-O(4) contacts which might have led to chain methyl benzoate formation. The 3.42 Å C(1)-O(1) contacts spiral in the opposite direction and would not be expected to give chain decomposition.

squares plane through the acetylperoxy group above. The rms distance of these five atoms from the phenyl plane is

3.51 Å, and the closest contacts are between C(5) and O(1) (3.30 Å, *a*) and between C(3) and O(3) (3.45 Å, *f*). Figure 4 shows those neighboring atoms which lie near the plane of the benzyloxy group.

Two of the six short contacts in Table III involve the methyl carbon, C(1), and suggest interesting induced decomposition mechanisms which are, however, excluded by our product studies. Figure 5 shows three molecules related by the screw axis at  $a = -1/2$ ,  $c = -1/4$ . Attack by C(1) of a methyl radical on O(4) of the adjacent molecule, only 3.45 Å away along the arrows in Figure 5 (d), could trigger an induced chain spiraling along the screw axis to form methyl benzoate and release the acetoxy's carbon dioxide. Such a mechanism would of course predict both crossover in the formation of methyl benzoate from isotopically mixed crystals and ester formation through the carbonyl oxygen while, in each case, the contrary was observed. There is no evidence for such an induced mechanism in solution so it may not be surprising that it does not occur in the solid. Attack by the methyl radical on the O(1) carbonyl oxygen of the molecule in the opposite direction along the screw axis (3.42 Å, *e*) should lead to methyl acetate, a product which is not observed. Induced decomposition in the liquid phase involves attack by the methyl radical on the para carbon (C7) of an intact molecule.<sup>5</sup> Although C(1) is only 3.718 Å from C(7) of another molecule, and only 0.38 Å from the axis of its  $p_z$  orbital (see just to the right of center in Figure 3), no such attack occurs in the crystal. The environment of the acetoxy group is discussed further below and illustrated in Figure 12.

Of the two solid-state radical pair coupling reactions, that of methyl and benzyloxy to give methyl benzoate is the more remarkable because of its preference for bond formation through O(3) rather than through O(4). Neither the molecular conformation nor the crystal packing gives a clear indication of the source of this preference. C(1) is slightly closer to O(3) (3.624 Å) than it is to O(4) (4.067 Å), but the difference is less than 0.5 Å and, as shown in Figure 2, the carbon dioxide molecule stands directly between them. It would seem plausible that the methyl radical should skirt the carbon dioxide and attack O(4), contrary to experimental observations. Clearly further evidence is required to explain preferential attack at O(3). It is available from the EPR spectra of the radical pair intermediates in the reaction.

**Radical Pair EPR Spectra. Theory.** The theory relating to the EPR spectra of radical pairs has been discussed previously and is closely related to the theory of molecular triplets and biradicals and to that of the CIDNP phenomenon.<sup>16</sup> In a laboratory magnetic field which is large compared with the local fields due to nuclei and other electrons, the vector sum of all fields to which a particular free radical electron is exposed will lie quite near the direction of the laboratory field. Thus the unperturbed spin wave functions of the electron in the laboratory field,  $\alpha$  and  $\beta$ , are an excellent basis from which to calculate the electron's magnetic energy by first-order perturbation. This approach is obviously not appropriate when the laboratory field is not large compared with the perpendicular components of local fields which have not been averaged to zero by molecular motion. Thus the theory of EPR spectra for molecular triplets and strongly interacting biradicals in viscous or solid media is more complex than that for radical pairs separated by some distance.

The spin functions for a pair of independent doublet state radicals (1 and 2) in an applied magnetic field are  $\alpha_1\alpha_2$ ,  $\alpha_1\beta_2$ ,  $\beta_1\alpha_2$ , and  $\beta_1\beta_2$ , where, for example,  $\alpha_1\beta_2$  denotes spin  $\alpha$  on radical 1 and spin  $\beta$  on radical 2 in a two-electron Slater determinant. These states may or may not remain ap-

propriate as the radicals are brought to a distance where they begin to interact. The  $\alpha_1\alpha_2$  ( $T_{+1}$ ) and  $\beta_1\beta_2$  ( $T_{-1}$ ) states remain satisfactory because of their large and distinctive Zeeman energies, but the  $\alpha_1\beta_2$  and  $\beta_1\alpha_2$  pair-of-doublet states with similar Zeeman energies may be mixed to  $(\alpha_1\beta_2 + \beta_1\alpha_2)(2)^{-1/2}$  and  $(\alpha_1\beta_2 - \beta_1\alpha_2)(2)^{-1/2}$ , which are triplet ( $T_0$ ) and singlet ( $S$ ) states, respectively. This mixing is favored by phenomena which cause  $T_0$  and  $S$  to differ in energy,<sup>17</sup> such as (1) the electron-electron magnetic dipolar interaction which affects the energy of the triplet but not that of the singlet, (2) the ability of both electrons in the singlet to occupy the same low energy molecular orbital while one electron of the triplet must occupy a higher orbital, and (3) the reduced electron-electron repulsion in the triplet due to the antisymmetry of its two-electron spatial wave function. The mixing will be opposed by phenomena which cause  $\alpha_1\beta_2$  and  $\beta_1\alpha_2$  to differ in energy. Since these states differ in energy by the difference in EPR excitation energy of the two individual radicals, they will be kept distinct by factors such as (1) a difference in  $g$  factor or (2) a difference in hyperfine energy between the radicals of the pair.

The pair-of-doublet and singlet-triplet states give quite different EPR spectra. In  $S$  and  $T_0$ , each radical has identical occupancy by  $\alpha$  and  $\beta$  spin so there can be no net magnetic interaction either between electron and nuclear spins (no hyperfine splitting of these levels) or between electron spins and electron orbital moments (no  $g$  shift of these levels). Moreover, while the energies of both  $\alpha_1\beta_2$  and  $\beta_1\alpha_2$  include the same electron-electron magnetic interaction,<sup>18</sup> in the  $T_0$ - $S$  pair, only the former is influenced by this interaction, but by twice as much as either  $\alpha_1\beta_2$  or  $\beta_1\alpha_2$ .

For the pair-of-doublets state, there are two EPR patterns, each corresponding to absorption by one radical, centered with the appropriate  $g$  factor, and showing the "normal" electron-electron magnetic splitting ( $2D_{zz}$ ) and nuclear hyperfine structure.

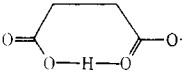
The singlet radical pair gives no EPR signal, but the triplet pair gives a single pattern which (1) is centered according to the average of the  $g$  factors for the component radicals, (2) shows half again as much electron-electron magnetic splitting ( $3D_{zz}$ ) as the pair-of-doublets, and (3) shows hyperfine coupling with the nuclei of both members of the pair, but with only half the normal spectroscopic splitting. Obviously more complex spectra are to be expected for cases intermediate between pure pair-of-doublets and pure triplet-singlet. The radical pairs of interest here are pure triplet-singlet, and the spectroscopic parameters must be interpreted accordingly.

Since these pairs certainly have very small exchange energies, the singlet pairs must have nearly the same geometry as the corresponding triplet pairs.

**Methyl-Phenyl Radical Pairs.** In 1968 Zubkov, Koritskii, and Lebedev reported observing the EPR spectrum of methyl-phenyl radical pairs (M-P) in irradiated single crystals of ABP at 77 K.<sup>19</sup> In other work, we have found that at least 90% of the M-P arises from secondary photolysis of a primary methyl-benzyloxy radical pair (M-B).<sup>4</sup> This contrasts with the direct photolysis of *tert*-butyl perbenzoate in solution where previous studies have suggested that not all carbon dioxide forms by way of benzyloxy radical.<sup>20</sup> Figure 6 presents the spectrum observed near  $g = 2$  for an ABP crystal mounted with its  $b$  axis perpendicular to the applied magnetic field and irradiated at 64 K for 6 min. Figure 7 shows a spectrum obtained under similar conditions with the crystal in a different orientation and only 15 sec irradiation.

These signals must be due to radical pairs. Splittings in excess of 100 G in carbon-hydrogen-oxygen systems are al-

Table IV. Experimental  $g$  Tensors for Acyloxy Radicals<sup>a</sup>

$\text{RCO}_2\cdot$	$g_{xx}$	$g_{yy}$	$g_{zz}$	$g_{\text{iso}}$	Ref
	2.0261 (3°)	2.0035 (3°)	2.0061 (10°)	2.0119	<i>b</i>
$\text{HOOCCH}_2\text{CH}_2\text{CO}_2\cdot$	2.019 (8°)	2.003 (7°)	2.006 (7°)	2.009	<i>c</i>
$\text{HOOC}-\text{C}\equiv\text{C}-\text{CO}_2\cdot$	2.0308	2.0045	2.0073	2.0139	<i>d</i>
$\text{C}_6\text{H}_5\text{CO}_2\cdot$	2.0228 (28°)	2.0041 (27°)	2.0082 (7°)	2.0117	<i>e</i>

<sup>a</sup>The principal values of the tensor are reported together with the deviation of the principal axes from the local pseudo-symmetry axes of the  $\text{CCO}_2$  group of the undamaged molecules which constitute the host. The  $y$  axis lies along the  $\text{CC}$  bond, the  $z$  axis is normal to the plane, and  $x$  is orthogonal to  $y$  and  $z$ . <sup>b</sup>M. Iwasaki, B. Eda, and K. Toriyama, *J. Am. Chem. Soc.*, **92**, 3211 (1970); B. Eda and M. Iwasaki, *J. Chem. Phys.*, **55**, 3442 (1971). <sup>c</sup>H. C. Box, H. G. Freund, K. T. Lilga, and E. E. Budzinsky, *J. Phys. Chem.*, **74**, 40 (1970). <sup>d</sup>H. Muto, K. Toriyama, and M. Iwasaki, *J. Chem. Phys.*, **57**, 3016 (1972). <sup>e</sup>Present work. Estimated error of  $g$  values  $\pm 0.0008$ . Direction cosines of the principal axes in the  $a, b, c^*$  coordinate system of ABP are:  $x$  (-0.1948, 0.4609, -0.8658);  $y$  (-0.9046, 0.2568, 0.3402);  $z$  (0.3791, 0.8495, 0.3670).

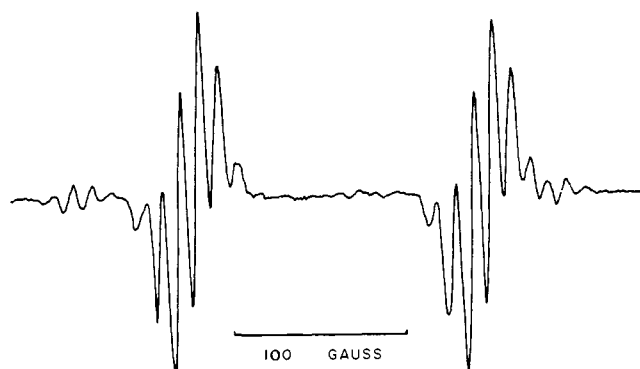


Figure 6. EPR spectrum of a single ABP crystal mounted with its unique  $b$  axis perpendicular to the applied field and irradiated for 7 min at 64 K.

most certainly due to the dipolar magnetic interaction of two electrons within less than 8 Å of one another. As discussed below, these large splittings show the anisotropy characteristic of electron-electron dipolar coupling. Only after much longer irradiation do signals appear which lack the large splitting and may be assigned to isolated methyl radicals.

The  $P2_1/c$  space group of ABP has four sites in the unit cell. These sites are related by inversion centers and twofold screw axes. Since electron-electron magnetic interactions are described by second-order tensors, which are invariant on translation or inversion but not on 180° rotation about an arbitrary axis, a certain radical pair species will give two different doublet splittings for a general crystal mounting, as in Figure 7 where one splitting is 204 and the other 86 G. One of these splittings is due to a family of radical pairs related by translations and inversions, while the other comes from a family of pairs related to the first by the screw axis. When the magnetic field is perpendicular to the screw axis, as in Figure 6, the magnetic interactions in all four sites are equivalent by symmetry, and different electron-electron splittings must be assigned to completely different species.

The stronger pair of signals in Figure 6, split by 171 G, corresponds to the spectrum previously assigned to M-P.<sup>19</sup> This assignment is supported by the hyperfine splitting pattern,<sup>19,21</sup> the nearly isotropic  $g$  factor,<sup>21</sup> the formation by photolysis of M-B,<sup>4</sup> and the quantitative agreement between the absolute intensity of this signal and the yield of toluene.<sup>4</sup>

**Methyl-Benzoyloxy Radical Pairs.** The weaker pair of signals in Figure 6 with a 277-G splitting corresponds to both pairs of signals in Figure 7 and has not been reported previously. It is due to a species which quickly builds to a low photostationary concentration, while M-P grows more slowly and to a much higher concentration. Thus a spectrum after short irradiation shows no M-P and only these

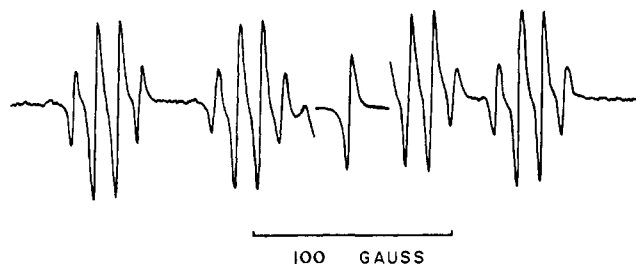


Figure 7. EPR spectrum of a single ABP crystal in a general orientation irradiated for 15 sec at 64 K. The central singlet is an internal DPPH polycrystalline standard and is recorded with 100 times less amplification than the rest of the spectrum.

signals, which we attribute to M-B on the basis of the following considerations.

(1) There are clean hyperfine quartets with a splitting which is isotropic within about 0.5 G and has an average value of 11.7 G. This is just half that of the free methyl radical, as would be expected for a triplet M-B pair with unresolvable hyperfine splitting by the benzyloxy protons.

(2) Irradiation of a crystal containing this radical pair at 67 K with an incandescent lamp causes quantitative conversion of the M-B signal to that of M-P.<sup>23</sup> Studies of the rate of this conversion as a function of intensity and wavelength in the range 550 to 1300 nm established that the efficiency per incident quantum is maximal at 750 nm and falls off gradually to a low value at 1300 nm.<sup>4</sup> Thus 750 nm corresponds to the long wavelength absorption maximum of benzyloxy radical if the quantum yield over this range is unity or at least constant. We had not anticipated that this electronic absorption should occur in a wavelength region including the near ir.

(3) Saturation of this EPR signal begins at 3 mW microwave power, while that of M-P begins at 0.03 mW. The shorter spin-lattice relaxation time of the M-B pair can be attributed to spin-orbit coupling in its oxygen-centered radical.

(4) Assuming that one of the radicals in the pair is methyl, which has a nearly isotropic  $g$  tensor, the  $g$  tensor of the other radical can be calculated from the experimental  $g$  tensor by subtracting  $g$  of methyl from twice the experimental tensor. The  $g$  tensor was determined experimentally from 67 EPR spectra of three irradiated ABP crystals in general orientations using a least-squares procedure described in the Appendix. Table IV shows that the principal values of the difference tensor are quite similar to those determined for supposed acyloxy radicals generated by X or  $\gamma$  irradiation of crystalline carboxylic acids at low temperature.<sup>24</sup> Moreover, the orientation of the tensor with respect to the benzyloxy portion of undamaged ABP corresponds to that for the other acyloxy radicals.

**Benzyloxy:  $\sigma$  or  $\pi$ ?** Observation of the benzyloxy radical as the M-B pair in crystalline ABP should allow deter-

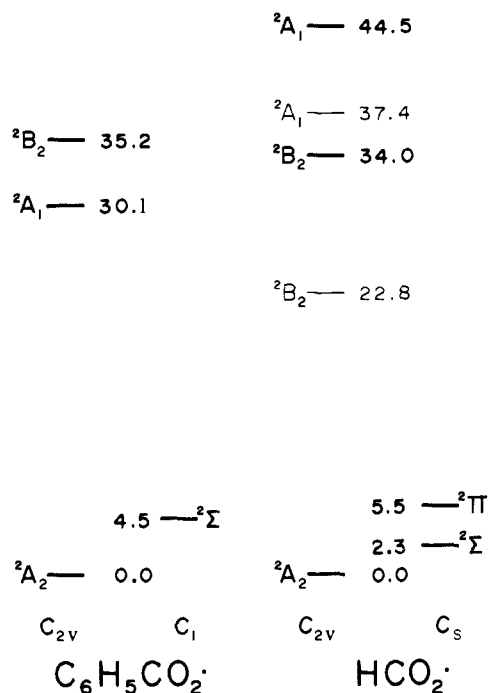


**Figure 8.** Relative energies (kcal/mol) calculated by INDO for various geometries and electronic configurations of the benzoyloxy and formyloxy radicals. The geometry of benzoyloxy is idealized in  $C_{2v}$  with  $\angle OCO = 120^\circ$ ,  $C-O = 1.29 \text{ \AA}$ . The  $C_1$  geometry was taken from the ABP crystal structure (Table I). For  $C_{2v}$  of formyloxy, the bold face entries are for the minimum energy geometry of the  ${}^2A_2$  configuration, the others are for individually energy-minimized geometries in this point group.<sup>35</sup> The  $C_s$  geometry is the energy minimum for the  ${}^2\Sigma$  configuration with  $\angle OCO = 124^\circ$ ,  $\angle HCO(1) = 109^\circ$ ,  $C-O(1) = 1.34 \text{ \AA}$ ,  $C-O(2) = 1.26 \text{ \AA}$ ,  $C-H = 1.12 \text{ \AA}$ .

mination of many chemical and physical properties of this important reaction intermediate.<sup>26</sup> The spin distribution in the radical is especially important to this paper but, since we have not yet measured it directly in ENDOR experiments, we have had to rely on atomic spin densities calculated semiempirically using INDO, the unrestricted SCF method of Pople.<sup>27</sup> In this connection, it is crucial to identify the electronic ground state of the radical. As in other radicals containing heteroatoms<sup>28</sup> there is a question whether benzoyloxy is a  $\sigma$  or a  $\pi$  radical.  $\sigma$  ground states have been assigned to other acyloxy radicals on the basis of their  $g$  tensors,<sup>29</sup> but we show below that reliable qualitative interpretation of these  $g$  tensors is far from simple. Similarity among the tensors of Table IV may suggest that most acyloxy radicals have the same ground state, and we favor a  $\pi$  state for benzoyloxy on the basis of INDO, ab initio STO-3G, and  $C^{13}$  CIDNP evidence.

**INDO Calculations.** We carried out INDO calculations on benzoyloxy for an idealized  $C_{2v}$  geometry with C-O bond lengths of  $1.29 \text{ \AA}$  and  $120^\circ$  bond angles and for the  $C_1$  geometry of the benzoyloxy atoms in intact ABP with unequal C-O bond lengths and C-C-O angles (see Figure 1). In the first geometry, we used a procedure analogous to that of ref 28b to calculate the lowest energy configuration of each symmetry  ${}^2A_1$ ,  ${}^2A_2$ , and  ${}^2B_2$  (the lowest  ${}^2B_1$  configuration is an excited  $\pi$  radical and would be much higher in energy). Only one SCF configuration could be calculated for the second geometry since its point group is  $C_1$ . The relative energies calculated for these single-determinant states are presented in Figure 8. The form of the lowest vacant orbital in each case is like one of those shown in Figure 9 for  $HCO_2$ . It is remarkable, but perhaps fortuitous, that the calculated vertical energy gap between the  $\pi$  ground configuration and the  $\sigma$  excited ones matches the broad, long

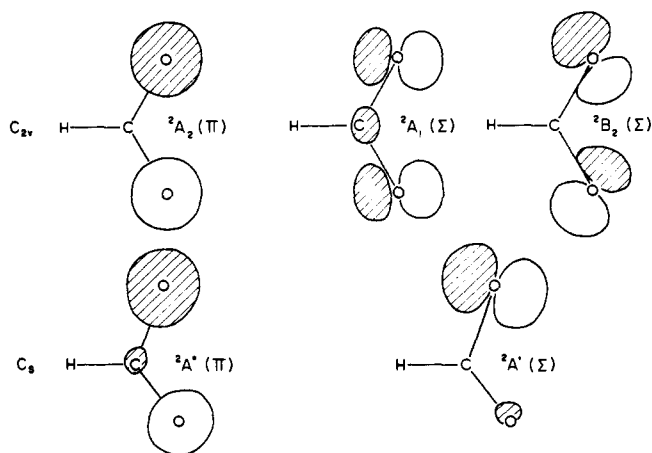


**Figure 9.** Lowest vacant INDO orbital for several electronic configurations of two geometries of the formyloxy radical.  $\sigma$  orbitals are outlined at  $0.15 \text{ au}$  in the molecular plane.  $\pi$  orbitals are outlined at  $0.1 \text{ au}$  at  $0.3 \text{ \AA}$  above the plane.  $(\text{au})^2 = e/a_0^3$ .

wavelength absorption which leads to decarboxylation. On the basis of orbital symmetry arguments, one would predict that the  $\sigma$  state should be more prone than the  $\pi$  to decarboxylate.<sup>35</sup>

Since the nearly degenerate  $\sigma$  radical configurations will be mixed by  $B_2$  vibration (antisymmetric stretching) of the carboxyl group,<sup>30-32</sup> it is not surprising that the  $C_1$   $\sigma$  radical configuration is much lower in energy than the  $\sigma$  configurations of the  $C_{2v}$  radical. Especially since we did not search for the geometry of minimum energy for these configurations, we can have little faith in the magnitude, or even the sign, of the  $4.5 \text{ kcal/mol}$  separation between the distorted  $\sigma$  excited state and the  $\pi$  ground state calculated by INDO.

The half-filled orbitals of the  $C_{2v}$  configurations are more than 95% localized on the carboxyl group and the adjacent carbon, and the half-filled orbital of the  $C_1$  radical is 77% localized on the same atoms. This suggests that carboxyl radicals should be relatively insensitive to the substituent group (see Table IV) and that formyloxy would be a reasonable model on which geometrical optimization could be attempted for the various electronic configurations.

Such an attempt using INDO has recently been reported,<sup>35</sup> but the molecule was constrained to  $C_{2v}$  symmetry preventing the favorable mixing of the  $\sigma$  states. Besides confirming the findings of this previous work, we have also minimized the energy of the  $\sigma$  configuration of the planar  $C_s$  molecule to a value only  $2.3 \text{ kcal/mol}$  above that of the symmetrical  $\pi$  state of optimized geometry.<sup>36</sup> We also calculated the  ${}^2A_1$  and  ${}^2B_2$  configurations in the  $C_{2v}$  geometry which minimized the energy of the  $\pi$  configuration and the  $\pi$  configuration in the  $C_s$  geometry which minimized the energy of the  $\sigma$  configuration.

The relative energies calculated for these various configurations and geometries are shown in Figure 8. The remarkable similarity of the energy differences to those of benzoyloxy suggests that other acyloxy radicals also may be similar, and that it will be difficult to distinguish the ground state on the basis of energies calculated by INDO.

It is unlikely that more sophisticated single-determinant SCF methods will give much more significant results since Newton has encountered numerous difficulties in ab initio calculations of  $HCO_2$  with a minimal basis set at the STO-3G level. The spin-unrestricted eigenstates show an unusually large admixture of states of higher multiplicity, and the spin-restricted solutions have much higher energies than the unrestricted. The energies are also lower using "spatially unrestricted" orbitals which are not representations of the

molecular point group. For calculations with neither spatial nor spin restriction the  $C_{2v}$   $\pi$  configuration gave an energy lower than that of the distorted  $\sigma$  configuration, but the reliability of conclusions based on this difference is questionable.<sup>37</sup>

***g*-Tensor Ambiguity.** Shifts of the *g* factor from the free spin value of 2.0023 result from spin-orbit coupling. They depend on orbital angular momentum induced by the magnetic field, which mixes excited states into the ground state through *H*·*L*, the orbital Zeeman term. The *g* factor is diminished by contributions from excited states corresponding to configurations which differ from the ground state by promotion of the unpaired electron to a vacant orbital; it is increased by exchange of the half-vacancy among occupied orbitals.<sup>38</sup> Since all principal *g* values for acyloxy radicals are greater than 2.0023, we ignore the first type of excited state and consider only mixing among the configurations of Figures 8 and 9. It can easily be demonstrated using group theory that, since  $L_x$  transforms as  $B_1$ ,  $H_x$  will mix  ${}^2B_2$  with  ${}^2A_2$ . Similarly,  $H_y$  will mix  ${}^2A_1$  with  ${}^2A_2$ , and  $H_z$  will mix  ${}^2B_2$  with  ${}^2A_1$ . Since for each direction of the magnetic field, one state remains pure, one could hope to identify the ground state by the field direction which gives no *g* shift. That there is no such direction may mean the  $C_{2v}$  symmetry is at least slightly perturbed. The large value of  $g_{xx}$  makes it unlikely that the ground state is a close relative of the symmetrical  ${}^2A_1$  configuration.<sup>39</sup> The other configurations will be strongly coupled in pairs by  $H_x$ ,  ${}^2A_2$  with  ${}^2B_2$  and distorted  $\sigma$  with distorted  $\pi$ . If the  ${}^2A_1$  state were close in energy to a ground  ${}^2B_2$  state, one would predict a large  $g_{zz}$ . It is risky to exclude  ${}^2B_2$  from being the ground state on this basis, because at its optimum geometry the splitting from the  ${}^2A_1$  state may be substantial, and the observed direction of minimum *g* is consistent with that expected for a  ${}^2B_2$  ground state. Without confidence in the calculated energies of the excited configurations and in the precise geometry of the trapped radical, it is not possible to choose the ground state on the basis of the *g* tensor and the INDO calculations, and certainly not on the basis of symmetry arguments alone.

**Carbon-13 CIDNP.** Where INDO calculations give similar energies for the various electronic configurations of benzoyloxy and formyloxy, they predict distinctive spin distributions. This is apparent from the calculated isotropic hyperfine coupling constants of the carboxyl carbon and the adjacent substituent atom shown in Table V. All configurations should have substantial negative spin density on the carbonyl carbon, but the  ${}^2A_1$  and distorted  $\sigma$  states are predicted to have large positive spin density on the substituent atom as well. In the case of benzoyloxy, hyperfine coupling of the quaternary aromatic carbon is nearly as large as that of the carboxyl carbon.

Cage coupling of benzoyloxy radical with methyl or phenyl radical has been important in several  $C^{13}$  CIDNP studies.<sup>40</sup> When the exchange interaction (*J*) of a radical pair is much larger than the difference in magnetic energy of the unpaired electrons on the two radicals, the CKO theory of CIDNP predicts that the relative net polarization of the different nuclei in a given product should be related linearly to their different hyperfine coupling constants in the spin-sorting radical pair.<sup>41</sup> Even for  $J = 0$ , the relationship is nearly linear over the range  $0 < a < 35$  G for  $C^{13}$  polarization in phenyl benzoate. In methyl benzoate, the polarization is nearly linear in *a* below 15 G but is less sensitive to *a* from 15 to 45 G. All investigators have found strong enhanced absorption for the carbonyl carbon. For methyl benzoate, this enhancement is somewhat less than that of the methyl carbon. Since the relaxation time of the carbonyl carbon is longer than that of the methyl carbon, the *a* of the carbonyl

Table V. Isotropic Hyperfine Coupling Constants from INDO (Gauss)

Point group configuration	$C_6H_5CO_2$		$HCO_2$	
	$a_C^a$	$a_C^b$	$a_C$	$a_H$
$C_{2v}$				
${}^2A_2$	-22.4	4.5	-24.6	7.1
${}^2A_1$	-25.7	21.9	-32.0	127
${}^2A_1^c$			-34.5 <sup>d</sup>	168
${}^2B_2$	-42.6	0.7	-34.5	0
${}^2B_2^c$			-9.3	0
$C_1$				
${}^2\Sigma$	-14.1	12.7		
$C_s$				
${}^2\Sigma$			-24.6	43
${}^2H$			-23.8	6.5

<sup>a</sup> Carbonyl carbon. <sup>b</sup> Substituted phenyl carbon. <sup>c</sup> Geometry of minimum energy for this configuration and point group, see ref 35. <sup>d</sup> In ref 35, this constant was mistakenly reported as 172 G. Professor Koenig informs us that this was the calculated proton coupling and that the calculated carbon coupling was -35.8 G.

carbon in the benzoyloxy radical must be substantially less than the 41 G of the methyl radical. No one has found emission for the quaternary aromatic carbon.<sup>42</sup> We thus feel that neither the  ${}^2A_1$  nor the distorted  $\sigma$  configuration is the ground state of benzoyloxy radical in solution.<sup>43</sup>

While we have not been able rigorously to exclude the symmetric  ${}^2B_2$   $\sigma$  configuration, we prefer to agree with the INDO and ab initio calculations that the ground state of benzoyloxy in the M-B pair is the symmetric  ${}^2A_2$   $\pi$  state. If it were a *symmetric*  $\sigma$  state, our subsequent discussion would not be much affected since the INDO spin densities by atom are similar for all  $C_{2v}$  states.<sup>44</sup>

***D*-Tensor Theory.** The spin-spin magnetic energy from the interaction of two electrons depends on their spatial relationship and on their relative magnetic orientations. When the laboratory magnetic field is large, this energy may be treated as a first-order perturbation of the radical-pair spin states discussed above. The energy for a given spin state is then a simple function of the direction of the laboratory field (which fixes the magnetic direction of the electrons) in the molecular or crystal coordinate system (to which the spatial relationship of the electrons may be referred). The energy can be expressed as  $S \cdot D \cdot S$ , where *S* is the sum of the electron spin vectors for the two radicals and *D* is a symmetric, traceless tensor.

The elements of *D* depend on the spin distribution in the radical pair according to eq 1.<sup>16</sup> Since the averages in eq 1

$$D_{ij} = \frac{1}{2} g^2 \beta^2 \left\langle \frac{r^2 \delta_{ij} - 3r_i r_j}{r^5} \right\rangle \quad (1)$$

involve the distance between electrons (*r*) and the *x*, *y*, and *z* components of this distance ( $r_i$ ;  $i = x, y, \text{ or } z$ ), the *D* elements are dependent on electron correlation. For radical pairs, the correlation can be handled easily by assuming that one odd electron is on each radical. This assumption is reasonable since configurations with both odd electrons on the same radical correspond to ionic states which not only are coulombically unfavorable, but also, when triplet, must have one electron in an excited orbital of the anionic radical.

Given a set of atomic orbital spin densities and the atomic positions for each radical, *D* can be estimated by replacing the integrals implicit in eq 1 with sums over all interradical pairs of atoms, multiplying each geometric term by the positive or negative product of the spin densities of the two atoms.

Since the EPR fine structure splitting is  $3D_{zz}$ ,<sup>45</sup> the five independent elements of *D* may be determined experimentally by measuring this separation for five or more direc-

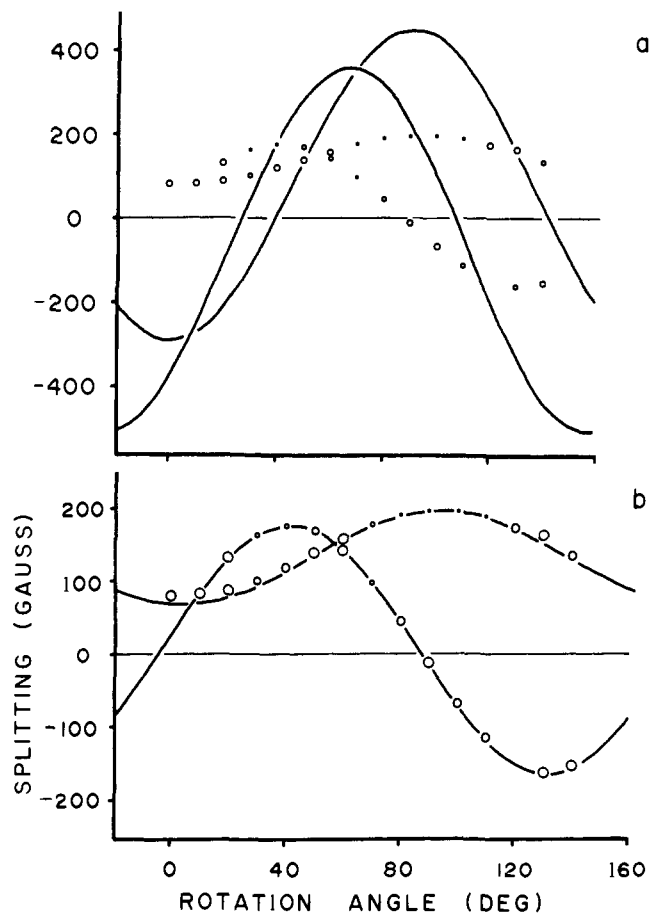


**Figure 10.** Calculated and experimental fine-structure splittings for the two symmetry-related M-B pairs in one general mounting of an ABP crystal. Solid lines are theoretical splittings (a) using tensor calculated from atomic positions of undamaged ABP and (b) using tensor fitted to experimental tensor by adjusting methyl position only. Estimated experimental error indicated by circle size. This crystal mounting includes 3 of the 8 observations in poorest agreement with the fitted tensor among 134 observations on 5 mountings.

tions of the magnet's field. These five values contain all the information on electron distribution which is available from such measurements.

In using the experimental  $D$  tensor to study the geometry of radical pairs, it is important to appreciate the experimental significance of the five items of information it contains. For some particular direction of the magnet's field, the dipolar splitting has its largest absolute value. The direction is described by two angles in the crystal coordinate system. These angles and the size of the splitting constitute three of the five items of information. If the splitting is not very sensitive to the direction of the magnet's field, the direction of maximum splitting is difficult to determine, and the angular information is of low quality. When the magnet's field is rotated in the plane perpendicular to this direction, some phase of rotation will give a larger splitting than any other (except for the identical splitting  $180^\circ$  away). The size of this second splitting, which will be of opposite sign from the first, and the phase of rotation in which it is observed are the remaining two items of information available experimentally. The smallest splitting observed with the magnet's field in the plane occurs at  $90^\circ$  from the largest and contains no additional information since the sum of splittings in three orthogonal directions must be zero. Customarily the difference between the largest and smallest splittings for the field in the plane is reported rather than the size of the largest. To the extent that this difference is very small, informa-

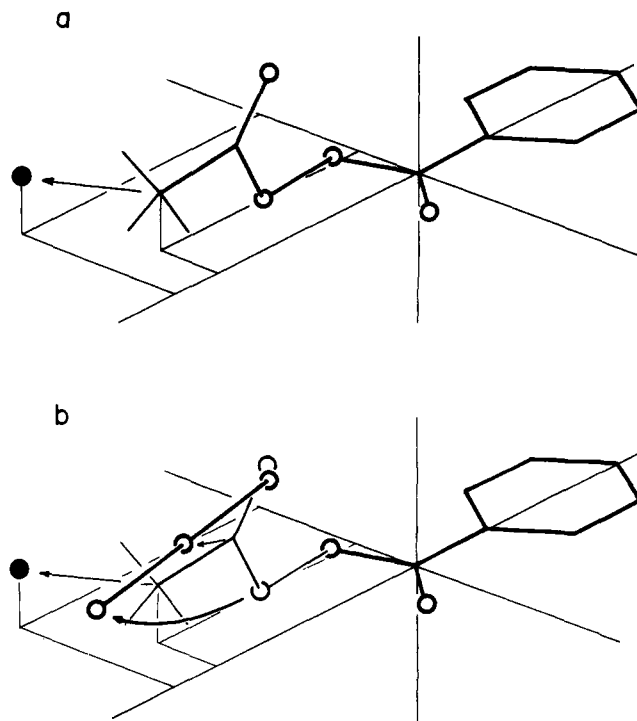


**Figure 11.** Perspective views of motion in the M-B pair relative to the undamaged ABP molecule. (a) Methyl motion inferred from  $D$  tensor assuming stationary  $\pi$ -benzoyloxy radical. (b) Methyl motion with  $\text{CO}_2$  motion inferred from hard-sphere packing analysis.

tion about the phase of rotation is poor.<sup>46</sup> These three directions are the principal axes of the  $D$  tensor, and its principal values are one-third of the corresponding spectral splittings.

**The Methyl-Benzoyloxy  $D$  Tensor.** Fine structure splittings were measured for five crystal mountings each rotated through  $180^\circ$  in steps of  $10^\circ$ . The magnetic field orientations completely spanned a unique set of directions in the crystal. This is helpful because the principal values of  $D$  are measured most sensitively near its principal axes, while the orientation is measured most sensitively between the axes, where the splitting changes rapidly with field direction. For most field directions, two splittings could be observed for the symmetry-related sets of M-B but, for some directions, spectral overlap made one or both splittings difficult to measure. In all, 134 measurements were made, 68 of one M-B family and 66 of the other. The five independent  $D$ -tensor elements were fit by linear regression to the measurements for each family separately and then, making use of the twofold rotation, to the combined data set. The splittings were given signs during the fitting process on the assumption that the largest should be negative. In fitting to the complete data set, 5 of 15 crystal mounting angles were corrected by less than  $2^\circ$  each to bring the splittings for the symmetry-related families within each of three crystal mountings into better agreement with a common  $D$  tensor. The observed splittings ranged from  $-346$  to  $+196$  G and gave a weighted rms deviation of 2.5 G from those calculated using the fitted tensor. The analogous deviation from a tensor that was fitted to the data without the condition that it be traceless was 1.4 G. While this improvement is statistically significant beyond the 99.99% confidence level,<sup>47</sup> the largest difference between corresponding elements of this tensor and the traceless tensor, both in diagonalized form, is 0.46 G or 0.3%, which is nearly within the estimated error.

Table VI presents the results of these four refinements. Since the tensors based on each of the two symmetry-related families and on a second set of crystals were determined almost completely independently, their differences can be



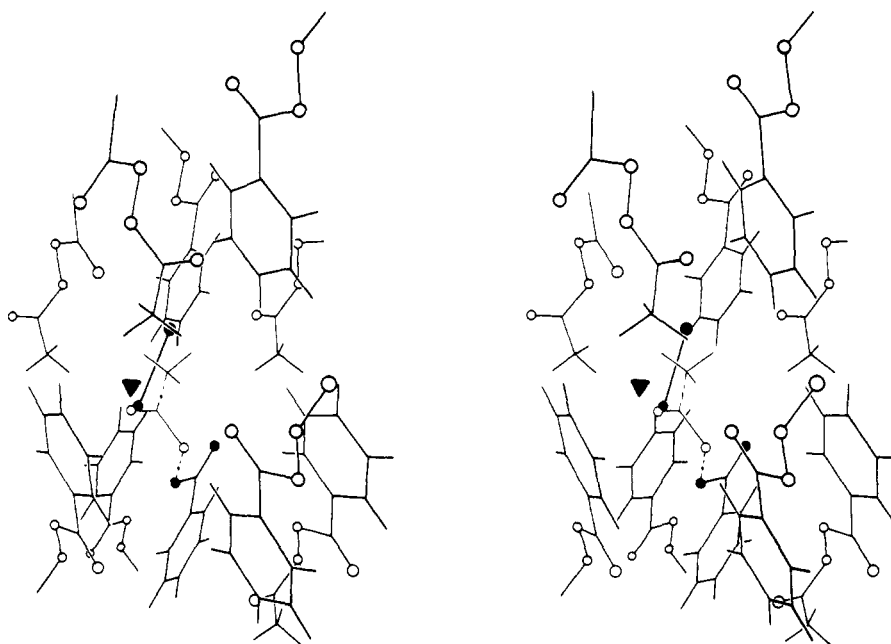


**Figure 12.** Stereo pair view of the M-B pair trapped in an undisturbed matrix of ABP molecules. The view is along the  $c^*$  axis with the  $b$  axis pointing right and  $a$  down. Circles denote oxygen atoms: those of the benzyloxy radical and of carbon dioxide are filled. The methyl radical's carbon atom is shown by a triangle. Note how the phenyl, methyl, and benzoyl groups in the foreground prevent the methyl radical from moving further toward the viewer. The original positions of methyl and carbon dioxide in intact ABP are included for reference with the breaking bonds dashed.

taken as a measure of the experimental error. This would suggest that the direction of maximum splitting is known within  $\pm 0.3^\circ$ , that the phase of rotation of the tensor about this direction is known within  $\pm 3^\circ$ , that the largest fine-structure splitting is  $-374 \pm 2$  G, and that the difference between the splittings in the other principal directions is  $22 \pm 4$  G.

**Interpretation of the  $D$  Tensor.** Assuming the atomic orbital spin densities given by INDO for the  $\pi$  benzyloxy radical, one could hope to use the  $D$  tensor to determine the radical-pair geometry, but the five experimental numbers are inadequate to fix the coordinates of so many atoms. Even assuming a rigid benzyloxy radical of known internal geometry and an axially symmetric methyl radical, three numbers are required to specify the vector between the radicals and five more to specify their angular orientation. Lacking more detailed information, such as might be provided by ENDOR, we can only test various models for their agreement with the experimental tensor.

It is easy to show that the model with the spin density of each atom of the radical pair at the location of the corresponding atom in undamaged ABP is not realistic. The principal values of the  $D$  tensor calculated from this geometry are more than twice too large, and the principal axes deviate from the observed directions by from 7 to  $21^\circ$  (see Table VI and Figure 10a).

A somewhat more sophisticated model allows the methyl radical to move while holding the atoms of the larger benzyloxy radical at the locations they occupy in undamaged ABP. This model allows adjustment of only the three cartesian coordinates of the methyl radical so, with five experimental observations, the solution is overdetermined. We calculated the position of the methyl radical which minimizes the sum of squared differences between calculated and observed  $D$  tensor elements. With the methyl radical in its optimum location the calculated and observed  $D$  tensors agree almost within the experimental error (See Table VI and Figure 10b). The largest fine-structure splitting was matched within 1.6 G, and the range of splittings in the perpendicular plane was matched within 1.5 G. The direction

**Table VI.** Experimental and Calculated  $D$  Tensors

Rms deviation, <sup>a</sup> Gauss	Principal values, Gauss			Axis orientation, <sup>b</sup> deg			
	$D_{xx}$	$D_{yy}$	$D_{zz}$	$x$	$y$	$z$	
Experimental <sup>c</sup>							
Ia	2.5	-125.0	66.2	58.8			
Ib	2.2	-125.5	66.6	58.8	0.2	0.7	0.8
Ic	1.6	-124.5	65.3	59.3	0.2	5.4	5.4
Id	1.4	-124.5	66.4	59.0	0.2	1.5	1.5
Ila	1.1	-124.0	66.1	58.9	0.4	3.8	3.8
Calculated <sup>d</sup>							
Stationary atoms		-277.1	156.0	121.1	21.9	7.2	21.3
Adjusted methyl		-125.0	66.2	58.8	1.9	1.8	0.6

<sup>a</sup>  $[\sum w(S_o - S_c)^2 / \sum w]^{1/2}$ , where  $w$  is the weight assigned to observed splitting  $S_o$ ,  $S_c$  is the calculated splitting, and the sum runs over all observations. Divide by 3 to compare with  $D$  errors. <sup>b</sup> Angular deviation from the corresponding principal axes of Ia. The direction cosines of these axes in the  $a, b, c^*$  coordinate system of ABP are:  $x$  (0.4296, 0.3565, -0.8297),  $y$  (0.3565, 0.7772, 0.5186),  $z$  (0.8297, -0.5185, 0.2067). <sup>c</sup> Ia, traceless tensor fit to 134 observations of both symmetry-equivalent M-B pairs on fine crystals. Ib, same as Ia with 68 observations for one pair. Ic, same as Ib with 66 observations for the other pair. Id, all 134 observations of Ia fit to a nontraceless tensor. Ila, exact refinement from 67 observations of both M-B pairs of three crystals in a different series of experiments. <sup>d</sup> First entry based on X-ray atomic coordinates and INDO  $^2A_2$  atomic spin densities for the benzyloxy radical. Second entry based on a similar calculation in which the methyl position is adjusted to give the best least-squares agreement between the calculated tensor and experimental tensor Ia.

of the principal axis with the largest splitting was matched within  $0.05^\circ$  and those of the other axes within  $0.2^\circ$ . The optimized methyl position is 2.38 Å from the position of C(1) in the precursor ABP molecule along a direction nearly parallel to the C(3)-O(3) bond as shown in Figures 11a and 12. The motion of the methyl group of the top molecule in Figure 3 would be toward the phenyl group beneath it.

The surprising success of this algebraically overdetermined model tends to support its assumptions and requires

analysis of the sensitivity of the matching to details of the model. Although placing the spin density of an atomic orbital at the position of the nucleus should be a good approximation for radicals separated by more than 5 Å,  $\pi$ -orbital spin density might be more accurately simulated by placing half of that spin above and half below the atomic nucleus at a certain distance along the atom's  $p_z$  orbital.<sup>48</sup>

The distance which should be used in such a calculation is not obvious. The leading term in an expansion of the integral we would like to approximate involves  $z$  of one atom when the other atom in the integral lies along the  $z$  axis of the first, but it involves  $z^2$  when the second atom lies in the  $xy$  nodal plane. For the Slater  $2p_z$  atomic orbital of carbon, the square root of the expectation value of  $z^2$  is 0.691 Å, and the expectation value of  $z$  in one lobe of the orbital is 0.611 Å. The corresponding values for oxygen are 0.494 and 0.437 Å, respectively. Since most of the spin density in M-B is calculated to be in the  $\pi$  orbitals of the methyl carbon and the benzyloxy oxygens, we considered what effect extension of the model's spin density along the  $p_z$  orbitals would have on the calculated tensor.

The largest (negative) splitting of the M-B pair occurs when the magnet's field parallels the direction between the radicals. The existence of a difference between the two splittings measured with the field along the other two principal axes means that the spin density is not cylindrically symmetrical about the interradsical vector. This is expected because extension of spin density perpendicular to the direction of maximum splitting should be larger in the plane of the three atoms with high spin density than it is in the direction perpendicular to this plane. Further extension of spin density in the plane of the atoms would enhance the deviation from cylindrical symmetry, while extension in the direction normal to this plane would diminish it. Since the oxygen  $p_z$  orbitals are almost normal to the plane, extension of their spin density would diminish the calculated asymmetry, which is already slightly smaller than the experimental value. This effect could be counteracted by extension of the methyl carbon's spin density perpendicular to the interradsical vector and in the plane of the three atoms. Crowding of the methyl radical against the face of a neighboring phenyl ring makes it likely that its  $p_z$  orbital should lie in the appropriate direction. This can be seen in the lower left corner of Figure 12.

With each choice of an oxygen  $\pi$  extension in the range 0 to 0.49 Å is associated a greater methyl  $\pi$  extension of 0.28 to 0.58 Å which optimizes the agreement between experimental and calculated  $D$  tensors. The optimum position of the methyl carbon is not very sensitive to the  $\pi$  extension and changes by only 0.1 Å over the range considered. The phase of rotation of the  $D$  tensor about the interradsical axis is much more sensitive to the position of the oxygens than to the  $\pi$  extension, changing through only 5° with variation of the latter. Thus within narrow limits, the experimental  $D$  tensor fixes the relative position of the methyl and benzyloxy radicals and establishes the plane containing the atoms of high spin density.<sup>49</sup>

The experimental  $D$  tensor makes it unlikely that the  $\pi$  benzyloxy radical rotates very much from its initial position in ABP about an axis normal to its plane. Such motion would either bring the atoms of high spin density closer together and require the methyl radical to retreat still further to keep the dipolar splitting small, or bring them into a line and decrease the cylindrical asymmetry of the  $D$  tensor. Our data do not prove that the benzyloxy radical does not move in forming the pair, but significant translation without reorientation seems unlikely. In the following discussion, we assume that only the methyl moves.

**Analysis of M-B Geometry.** The methyl radical position in the M-B pair is about 2.4 Å from its position in the ABP molecule (Figure 11). This surprisingly large displacement would clearly be impossible without cooperative motion of several neighboring molecules. Otherwise the methyl carbon would be only 2.6 Å from C(1) of the molecule across the center of symmetry at  $(-\frac{1}{2}, 0, 0)$  and only 3.4 Å from O(4) of the molecule related by the  $(x, \frac{1}{2} - y, \frac{1}{2} + z)$  glide. The worst collision would be with the para carbon of the phenyl ring against which the acetoxy group lay before decomposition. This distance would be only 2.1 Å without phenyl motion, and three other carbons of the phenyl ring would be within 3.2 Å of the new methyl position. While there might be a weak bonding interaction between the methyl radical and the phenyl group, spin density is not redistributed enough to alter the methyl hyperfine coupling or to give rise to observable splitting by the phenyl protons. How these three molecules hold the methyl radical can be seen in the foreground of Figure 12.

The new position of the methyl radical in itself suggests an explanation for preferential attack at O(3) of the geminate benzyloxy radical. In the starting material, C(1) is only 0.4 Å closer to O(3) than to O(4) but, in the radical pair, this difference increases to about 1.2 Å. If there were an attractive interaction between the methyl radical and the phenyl group at the lower left of Figure 12, one could also imagine a mechanism in which methyl glides along the face of the phenyl until it reaches O(4) of the benzyloxy radical. However, it seems likely that the most significant influence in radical coupling comes from the carbon dioxide molecule, the atoms of which lie between the methyl group and O(3) in intact ABP.

For the methyl radical to move so far toward the neighboring molecules, it must be pushed hard. The source of this push is almost certainly the carbon dioxide molecule, which becomes subject to van der Waals repulsion from the two radicals to which it was originally bonded. Although the EPR experiment does not provide direct information on the location of the carbon dioxide molecule, sites large enough to accommodate it can be selected on the basis of the probable positions for methyl and benzyloxy radicals and the assumption that neighboring molecules are stationary. The naivete of this assumption and uncertainty in the form and parameterization of equations for calculating van der Waals energies combine to make the precision of a calculated carbon dioxide location suspect, but simple calculation should give a reasonable approximation of the true geometry.

We first used a set of "soft" 6-12 van der Waals parameters<sup>50</sup> to map the energy of a carbonyl oxygen atom through the region where the carbon dioxide molecule might lie. The region within which its van der Waals energy was no more than 1.5 kcal/mol above the minimum value was large enough to allow a number of orientations for a linear carbon dioxide molecule 3.32 Å long. The allowed orientations had one oxygen near the initial location of O(1) and the other two atoms near the original acetoxy plane.

We then generated a more restrictive map based on hard-sphere potentials. There was only one orientation for linear carbon dioxide such that all its atoms would be more than 2.5 Å from neighboring hydrogens<sup>51</sup> and more than 2.8 Å from other carbon and oxygen atoms. This position for the carbon dioxide is illustrated in Figures 11b and 12. Although O(1) is displaced from its initial position by only 0.3 Å, O(2) has moved by 3.6 Å. This motion must result from repulsion between O(2) and O(3) when their bond is broken.

We cannot be certain whether the carbon dioxide mole-

cule is released during homolysis of the O(2)–O(3) bond of photoexcited ABP or whether it arises from decarboxylation of an intermediate acetoxy radical.<sup>52</sup> Our kinetic studies have shown that, if an intermediate precedes M–B, it must have a half-life of less than half a second at 77 K.<sup>4</sup> Whether the methyl group at first remains bonded to the carbon dioxide or not, it must move aside as O(2) swings back from O(3). In this process, the carbon dioxide which initially lay between C(1) and O(3) passes between C(1) and O(4) and ultimately lodges in a position which interferes with the methyl radical's approach to O(4) but leaves access to O(3) relatively free.

### Conclusion and Caveat

There may be as many as three factors which contribute to the observed discrimination in methyl benzoate formation during photolysis of crystalline ABP: (1) the methyl radical is closer to O(3) than to O(4) of the benzoyloxy radical, (2) the new carbon dioxide molecule screens O(4), and (3) weak bonding with the neighboring phenyl group may help steer the methyl radical to O(3).

These qualitative conclusions are much more reliable than the detailed geometric picture that was developed above. The weakest link in the geometric argument is our assumption of a  $C_{2v}$ -like spin distribution for the benzoyloxy radical. Minor changes in the atomic coordinates of these atoms would, in themselves, result in only minor corrections to the calculated positions of the methyl radical and carbon dioxide molecule. But if this minor variation in atomic positions resulted in major spin redistribution (most dramatically by giving a  $\sigma$  ground state with 95% of the spin density on the "single-bonded" oxygen atom), then the calculated methyl and carbon dioxide positions would change drastically. We have carried out a  $D$ -tensor analysis assuming a  $C_1$   $\sigma$  benzoyloxy radical and have reached the same qualitative conclusions as above, although the methyl radical motion is smaller in this case.

Even if the benzoyloxy radical is a  $C_{2v}$   $\pi$  radical in solution, the INDO calculations suggest that it may be malleable enough to be distorted by lattice forces. One warning that the benzoyloxy radical geometry may differ from the one we have assumed is the orientation of the experimental  $g$  tensor (Table IV). Although one principal axis is satisfactorily perpendicular to the assumed plane of the radical, the others diverge from the pseudo-symmetry axes by more than 25°. This divergence is in the wrong direction to be consistent with an unmoved  $\sigma$  radical and suggests some rotation of the benzoyloxy radical within its plane. There is a clear need for magnetic double resonance work to determine the geometry and spin distribution of this radical.

Another puzzling observation is that the methyl radical of the M–P pair appears to be closer to its initial location in intact ABP than does the methyl radical of the M–B pair.<sup>40c</sup>

In rationalizing the oxygen discrimination, we have ignored the more prevalent scrambling process. The higher discrimination in an ethanol glass could be attributed to hydrogen bonding, but we suspect that scrambling in the crystal might be due to the coexistence of two or more specific and noncompeting pathways<sup>54</sup> among which only one gives the trapped M–B pairs we can observe by EPR.

The absence of induced decomposition in spite of apparently favorable positioning of the methyl radical suggests that higher temperature studies with less mobile radicals would be necessary to study this type of radical–molecule chain process in such crystals.

The structural and dynamic aspects of this problem are under continuing investigation.

### Experimental Section

**Instrumentation.**  $^1\text{H}$  NMR spectra were recorded on Jeolco Minimar-100 and Varian A60, A60-A, and HA-100 spectrometers. Mass spectra were determined at 70 eV on an AEI MS-9 and on a Hitachi Perkin-Elmer RMU-6 equipped with a Perkin-Elmer 990 gas chromatograph inlet. Analytical gas chromatography used a Hewlett-Packard-F & M 4241 with flame ionization detector. Ultraviolet spectra were recorded with a Bausch and Lomb/Shimadzu UV-200 and infrared with a Perkin-Elmer 421. X-Ray diffraction measurements were made with a Picker FACS-I diffractometer system using pulse height discrimination and Mo  $K\alpha$  radiation isolated by a graphite monochromator. EPR spectra were recorded on a Varian E-9 spectrometer operating at X band with 100 kHz detection. Differential scanning calorimetry was performed with a Perkin-Elmer DSC-1b. Elemental analysis was by Atlantic Microlabs, Atlanta, Ga.

**Acetyl benzoyl peroxide (ABP)** was prepared by autoxidation of benzaldehyde (10.6 g) in acetic anhydride (30 g) containing anhydrous sodium acetate (1 g).<sup>55</sup> Several times during 6 hr of stirring under oxygen, the solution was irradiated briefly with a GE sunlamp. When 80% of the theoretical oxygen had been absorbed, acetic acid and remaining acetic anhydride were removed by bulb-to-bulb distillation at  $10^{-3}$  Torr. The residue was dissolved in ether washed with a small amount of water and recrystallized from ether–pentane (1:1) at Dry Ice temperature. The 9.1 g of colorless crystalline ABP was 99.8% pure by iodometric titration in ethanol: mp 36.5–37.5° (lit.<sup>5</sup> 38°);  $^1\text{H}$  NMR ( $\text{CCl}_4$ )  $\delta$  2.16 (s, 3), 7.40 (m, 3), 7.86 (m, 2); uv (cyclohexane)  $\lambda_{\text{max}}$  228 nm ( $\epsilon$  12,300), 274 (1050), 281 (859) with tailing into the visible such that: 302 nm ( $\epsilon$  5), 313 (2), 334 (1), 366 (0.4), and 406 (0.2); MS (70 eV)  $m/e$  180 (26.6, M+), 123 (6.7), 122 (86.6,  $\text{PhCO}_2\text{H}^+$ ) 106 (27.1), 105 (100,  $\text{PhCO}^+$ ).

**ABP- $d_8$**  was prepared by an analogous reaction from benzaldehyde- $d_6$ , acetic anhydride- $d_6$ , and sodium acetate- $d_3$ . The benzaldehyde prepared by oxidation of toluene- $d_8$  (99%, Diaprep, Inc.) with cerium(IV) nitrate in 6  $N$  perchloric acid<sup>57</sup> was shown by MS to have  $d_8:d_7$  aldehyde- $h:d_7$  ring- $h:d_6$  = 90:3:4:3 and was used as a crude mixture with 25% of benzyl alcohol and benzoic acid. The acetic anhydride was prepared from acetic acid- $d_8$  (99% Diaprep, Inc.) via acetyl chloride and sodium acetate by standard methods.<sup>58</sup> The autoxidation was sluggish, and the yield of recrystallized peroxide was only 21% based on aldehyde. The MS was consistent with 93% ABP- $d_8$ , 7% ABP- $d_7$  with incomplete deuteration in the aromatic ring as expected from the aldehyde analysis:  $m/e$  189 (4.3), 188 (41, M- $d_8^+$ ), 187 (3.0), 129 (18), 127 (86,  $\text{C}_6\text{D}_5\text{COOD}^+$ ), 126 (6.9), 112 (3.5), 111 (29), 110 (100), 109 (63), 108 (4.3).  $^1\text{H}$  NMR ( $\text{CCl}_4$ ) displayed a weak peak at  $\delta$  7.83 in addition to small impurity absorptions from pentane solvent.

[ $^{18}\text{O}_2$ ]ABP with both peroxy oxygens labeled was prepared by an analogous autoxidation using  $^{18}\text{O}_2$  (98.6%  $^{18}\text{O}$ , 0.94%  $^{16}\text{O}$ , Miles-Yeda) which was introduced into the evacuated reaction flask by a Toepler pump. The recrystallized yield was 62% based on 94 ml of absorbed oxygen.

Incorporation of label was assayed shortly after synthesis by the mass spectrum of oxygen derived by acidic permanganate oxidation on the vacuum line of the aqueous perchloric acid hydrolysate (2.2  $N$  perchloric acid, 40°, 5.5 hr) of the ABP.<sup>59</sup> This MS had  $\text{O}_2$   $m/e$  36:34:32 = 95:2.8:2.2 while oxygen recovered from the oxidation mixture had the  $\text{O}_2$  isotopes in the proportion 93:2.6:4.2, suggesting slight contamination by atmospheric oxygen in handling, probably during analysis. After some months of storage at 0°, the label was analyzed by a modified technique involving base then acid hydrolysis before oxidation.<sup>60</sup> This experiment showed increased  $\text{O}_2$ -34 (36:34 = 93.8:6.2), suggesting minor scrambling during hydrolysis by this procedure (or, less likely, during storage). Simultaneously a sample of ABP recovered after 3% photolysis at –70° with 254-nm light was hydrolyzed and oxidized by the same method and gave an oxygen 36:34 ratio of 93.7:6.3.

**Photolyses** were conducted on samples sealed in narrow quartz tubes (after degassing at  $<10^{-3}$  Torr) and held in the broad quartz tip of a Dewar vessel containing ice–water (0°C), Dry Ice–ethanol (–65 to –70°C), or liquid nitrogen (77 K). Three lamp systems were used: A, 4 GE germicidal lamps (254 nm); B, a Rayonet Type R5 preparative reactor (254 nm); C, an Osram 200-W super-pressure Hg arc. A and B were used for solid photolysis and C for

solution photolysis. At 254 nm, an ABP crystal  $3 \times 10^{-4}$  mm ( $\sim 300$  unit cells) thick would absorb 90% of the incident light, assuming the solution extinction coefficient. At 366 nm, half the light would pass through a crystal 0.7 mm thick. The crystals in our samples were needles about 0.01 mm thick so low overall conversion at 254 nm may correspond to relatively high conversion in the absorbing layer. This may account for some of the oxygen scrambling in methyl benzoate formation. Quartz NMR tubes were used for solution photolysis so that progress of the reaction to completion could be monitored. Solid photolyses were interrupted after low conversion and before the sample showed signs of congealing.

**Analytical Procedure.** If necessary after photolysis, residual ABP was titrated iodometrically, and the methyl benzoate and toluene were separated by extraction with pentane and water. In one case, the methyl benzoate was collected by GC and analyzed separately by MS. In all other cases, the isotope analysis was conducted by combined GC-MS. The  $m/e$  region of interest was scanned repeatedly with continuous chart flow so a plot of peak height vs. time could be prepared. Isotopic abundances were compared at the maxima of the respective curves to avoid problems from GC isotope fractionation. No corrections were applied for kinetic isotope effects on relative ion abundances, which are not negligible but tend to cancel in the comparisons we make.

**Methyl benzoyl carbonate** was prepared according to the general procedure of Tarbell and Longosz<sup>61</sup> by adding 9.5 g of freshly distilled methyl chlorocarbonate slowly to a stirred solution of 12.2 g of benzoic acid and 10.2 g of triethylamine in 250 ml of dry ether cooled in ice. After stirring for 0.5 hr, the mixture was filtered, washed, dried, and distilled to give 16.4 g of the product: bp 80° (0.3 Torr); <sup>1</sup>H NMR (CCl<sub>4</sub>)  $\delta$  3.88 (s, 3), 7.45 (m, 3), 7.97 (m, 2); ir (CCl<sub>4</sub>) 1805, 1795, 1185, 1155, 1080, 1045, 978 cm<sup>-1</sup>. Anal. Calcd for C<sub>9</sub>H<sub>8</sub>O<sub>4</sub>: C, 60.99; H, 4.48; O, 35.52. Found: C, 60.24; H, 4.60. Irradiating a degassed sample of this compound with lamp system A for 8 hr at -69 to -72°C led to no new signals in the <sup>1</sup>H NMR spectrum. Solid ABP is 10% decomposed by this treatment.

**X-Ray Study.** Colorless crystalline plates of ABP for X-ray and EPR investigation were grown from pentane in a flask suspended in 25 l. of water which was allowed to cool over 18 hr from 20 to about 5° in a cold room. They could be stored at 0° for 4 years without apparent degradation. Weissenberg photographs showed a monoclinic system with systematic absences  $0k0$  for  $k$  odd and  $h0l$  for  $l$  odd. The plates showed (100) and were elongated along [010]. For diffractometry, the crystals were mounted in 0.5 mm quartz capillaries into which a short 0.5 mm diameter copper wire had been sealed with Apiezon W wax. The crystal was held against the flat face of the wire by red cotton fibers, and the open end of the capillary was sealed with wax and epoxy cement. This assembly was mounted with epoxy cement on the cooling block of an AIRCO cryotip goniometer head. The copper wire and the air sealed in the capillary provided thermal contact between the crystal and the cooling block when the beryllium shroud was evacuated. The temperature of the cooling block was monitored using the thermocouple gauge of the OC12A Cryotip control panel. Lattice parameters at  $-90 \pm 5^\circ\text{C}$  were determined by a least-squares fit to the setting angles for 12 carefully centered reflections with  $30^\circ < 2\theta < 50^\circ$  using the average of positive and negative  $2\theta$  angles for Mo K $\alpha_1$  (0.70926 Å).<sup>62</sup> Rms deviation of the setting angles was 0.03°. Crystal data are: C<sub>9</sub>H<sub>8</sub>O<sub>4</sub>; mol wt 180.2; monoclinic;  $a = 8.403$  (3) Å,  $b = 7.489$  (4) Å,  $c = 14.025$  (7) Å,  $\beta = 97.18$  (3)°;  $V = 876.1$  Å<sup>3</sup>;  $Z = 4$ ;  $\rho_{\text{calcd}} = 1.37$  g/cm<sup>3</sup>;  $\mu(\text{Mo K}\alpha) = 1.11$  cm<sup>-1</sup>; space group  $P2_1/c$ . Comparison with lattice parameters determined less carefully during orientation for data collection suggests that the uncertainty in the reported parameters may be twice as large as the indicated standard deviation in the last digit estimated from the reciprocal matrix of the refinement.

For data collection, a plate 0.4 mm thick and 0.5 mm wide was cut to a length of 0.55 mm and mounted with [010] roughly coincident with the goniostat  $\phi$  axis. Data were collected over a unique quadrant of the reflection sphere in two shells  $1^\circ < 2\theta < 43^\circ$  and  $43^\circ < 2\theta < 43^\circ$  using an 0.25°/min  $\omega$  scan of 0.7° plus an  $\alpha_1\alpha_2$  dispersion correction. The  $\omega$  width of low angle reflections was 0.05°, but the detector slits were opened to give a width of 0.15°. Background was counted for 20 sec at each extreme of the scan. Temperature was held at  $-95 \pm 5^\circ\text{C}$  during data collection with

occasional deviations by another 5°. Twice collection was interrupted and the head warmed to 0° to blow out ice which had formed in the expansion coils. After each warming, the crystal orientation was redetermined, and standard reflections were found to have lost no intensity. The three standard reflections were each measured 38 times during data collection. The variation of their intensities was apparently random giving standard deviations from the means of 1.7, 2.1, and 4.9%. Of the 1388 independent reflections with  $(\sin \theta/\lambda) < 0.573$ , 200 were measured more than once and agreed within 3% in  $F$ . In particular there seemed to be no systematic variation in intensity with temperature fluctuations over the range indicated. Lorentz, polarization, and background corrections were applied to the data, equivalent reflections were averaged, and  $F$ 's were calculated assigning  $F = 1$  to the 120 reflections with zero or negative corrected intensity.<sup>63</sup> For least-squares refinement, the observations were weighted by a standard scheme<sup>64</sup> using 1.5% as the systematic error.

The nonhydrogen atoms were located in an  $E$  map based on the 132 reflections with  $E > 1.8$  phased by symbolic addition using a local variant of the "Auto" program of Dunitz et al.<sup>65</sup> After preliminary refinement, the hydrogen atoms were located in a difference map, and the structure was refined by full-matrix least-squares using one scale factor and anisotropic temperature factors for all nonhydrogen atoms. Isotropic thermal parameters were varied for all hydrogens, but positional parameters were varied only for the methyl hydrogens. Ring hydrogens were held in idealized positions 0.98 Å from the corresponding carbon atom.<sup>66</sup> Dimensioning of the least-squares program required that the parameters of two nonhydrogen atoms be held fixed in each cycle of refinement but, after two cycles, only two of 111 parameter changes were as large as three times the estimated error of the parameter so the refinement was not continued to convergence. When refinement was stopped,  $R_w = \Sigma w(|F_d| - |F_c|)/\Sigma w F_o^2)^{1/2}$  was 0.050,  $R = \|F_d - |F_c|\|/\Sigma |F_d|$  was 0.044, and the largest peak in a difference map corresponded to an electron density of 0.16 e/Å<sup>3</sup>. Table VII contains values of  $F_o$ ,  $F_c$ , and  $(F_o - F_c)/(w)^{1/2}$ ; see paragraph concerning supplementary material at the end of this paper. Atomic position and thermal parameters are presented in Tables I and II. The interatomic distances and angles and their errors were calculated using the 1971 version of ORFEE3 by W. R. Busing et al.

**EPR measurements** were made on single crystals of ABP cooled by immersion in boiling nitrogen in an insert Dewar vessel in the Varian E-231 Multipurpose Cavity. The quartz-tipped Dewar had a 175-ml silvered reservoir capped with a No. 12 rubber stopper machined to fit tightly and reproducibly. The stopper was drilled to hold a tube for evacuating the reservoir, a nitrogen vapor pressure thermometer, and, in the center, a ball joint, which served as a bearing for the goniometer rod. The temperature of the nitrogen was controlled by evacuating the reservoir to a pressure controlled by a Cartesian diver manostat. The temperature could be varied from near the freezing point of nitrogen [63.3 K (96 Torr)] to its boiling point at atmospheric pressure (77.4 K). The pressure was controlled within  $\sim 10$  Torr and the vapor pressure thermometer held constant within  $\sim 5$  Torr. The corresponding temperature ranges are  $\pm 0.08$  and  $0.04^\circ$  at 75 K,  $\pm 0.11$  and  $0.06^\circ$  at 70 K, and  $\pm 0.4$  and  $0.2^\circ$  at 65 K. While the liquid in the unsilvered quartz tail may not have been cooled by convection from the reservoir, frequent bubbling kept it from superheating, and the maximum difference in hydrostatic pressure was 20 cm of nitrogen or 12 Torr. A single filling with liquid nitrogen was adequate for an experiment of 1 to 4 hr depending on temperature and amount of irradiation.

For the most experiments, a crystal plate about  $1 \times 2 \times 0.2$  mm was mounted with a thin film of Dow-Corning high vacuum silicon grease on a flat surface ground near the end of a 3 mm diameter Suprasil quartz rod parallel to its axis. The top of the rod was fitted with a socket joint, which mated with the ball joint in the rubber stopper, and with a pointer which allowed measurement of angular displacement about the axis of the rod within  $0.5^\circ$  by reading on plastic polar graph paper cemented to a rectangular sheet of  $\frac{3}{8}$  in. Lucite attached to the rubber stopper. The dimensions of the Lucite rectangle were such that it just fit between the magnet coil housings of the EPR spectrometer allowing easy alignment.

Orientation of the crystal on the mounting rod is determined by three angles: the angle ( $\phi$ ) between the axis of the quartz rod and the normal to the plate face ( $a^*$ ), the angle ( $\theta$ ) between the axis of

the quartz rod and the optic axis ( $b$ ) in the plane of the crystal plate (100), and the dihedral angle ( $\chi$ ) between the pointer at the top of the rod and  $a^*$ . We measured  $\theta$  using a Bausch and Lomb Stereozoom 7 microscope with a protractor reticle. Since the long edges of the plates are parallel to  $b$ ,  $\theta$  could be measured within  $1^\circ$  on a well-formed crystal and within  $2^\circ$  on others. We could determine  $\phi$  and  $\chi$  more accurately by using light reflected from the plate face. The complete assembly without the Dewar was mounted 30 cm in front of a vertical white surface with the quartz rod vertical. A Nicholas microscope illuminator was positioned about 50 cm in front of and somewhat below the crystal so that the shadow of the crystal on the white surface fell 10 cm above the projection of the crystal on the surface. The observer then moved his head until with one eye he could see the glint of the lamp off the face of the crystal and read from a grid on the white surface the displacement of the image of the crystal from a point 10 cm below the projection of the crystal. A displacement of 1 cm corresponded to a  $1^\circ$  displacement of  $a^*$  so  $\phi$  and  $\chi$  could easily be determined within  $0.5^\circ$ .

The crystal was irradiated through the slotted grid of the cavity using light from an Osram HBO 200 W/2 mercury arc focused by an  $f/1$  quartz lens. Infrared light and light of wavelength less than 300 nm were removed by 5 cm of an aqueous solution of  $\text{CuSO}_4$  (100 g of  $\text{CuSO}_4 \cdot 5\text{H}_2\text{O}/\text{l}$ ). In some experiments, a Corning 7-54 glass color filter was used to remove visible light ( $>400$  nm), which causes the benzyloxy radical to decarboxylate. With or without the 7-54 filter, 366-nm light accounts for more than 90% of the absorption by ABP. The intensity of the light was uniform through the crystal since a negligible fraction was absorbed.

For determining the  $D$  and  $g$  tensors of the M-B pair, the crystal was irradiated for 10–20 sec at about 65 K. Spectra in many orientations could be recorded at that temperature before it was necessary to renew the radical pair by another short irradiation. Usually the total exposure of a crystal was less than 2 min, which would result in less than 0.01% decomposition. Fine-structure split-

$$\begin{array}{lll} [g_{zz}\beta H + D_{zz}/2] & [2^{-1/2}\{\beta H(g_{zx} - ig_{zy}) + D_{zx} - iD_{zy}\}] & [(D_{xx} - D_{yy})/2 - iD_{xy}] \\ [2^{-1/2}\{\beta H(g_{zx} + ig_{zy}) + D_{zx} + iD_{zy}\}] & [-D_{zz}] & [2^{-1/2}\{\beta H(g_{zx} - ig_{zy}) - D_{zx} + iD_{zy}\}] \\ [(D_{xx} - D_{yy})/2 + iD_{xy}] & [2^{-1/2}\{\beta H(g_{zx} + ig_{zy}) - D_{zx} - iD_{zy}\}] & [-g_{zz}\beta H + D_{zz}/2] \end{array} \quad (\text{A3})$$

tings were measured directly from calibrated chart paper. Field reproducibility was better than the thickness of the line drawn by the recorder; the sweep is reportedly<sup>67</sup> linear within about twice this value. Shifts in the  $g$  factor were measured relative to the signal of a speck of polycrystalline diphenylpicrylhydrazyl ( $g$  2.0037)<sup>68</sup> placed in the silicon grease next to the crystal.

**$D$  and  $g$  tensors** were refined from the fine-structure splittings and  $g$  shifts using programs written for the Wang 2200 calculator. Tables VIII and IX (see paragraph concerning supplementary material at the end of this paper) contain the observed fine-structure splittings and  $g$  shifts and the values calculated from the fitted  $D$  and  $g$  tensors. Model testing and drawing of the structural illustrations in this paper were also done with the help of this calculator.

**INDO calculations** were performed using versions of the Dobosh program (Quantum Chemistry Program Exchange No. 141) modified for the IBM 370-155 by R. B. Davidson and for the PDP11-45 of K. B. Wiberg by D. Raich and J. J. Wendoloski. Table X (see paragraph concerning supplementary material) presents the atomic spin densities calculated by INDO for benzyloxy radical in the  $C_{2v}$   $\pi$  configuration and in the  $C_1$   $\sigma$  configuration.

## Appendix

Aside from hyperfine structure, the results of EPR investigations of triplet-state organic molecules are usually consistent with an electron spin Hamiltonian of the form (A1)

$$H = \beta H \cdot g \cdot S + S \cdot D \cdot S \quad (\text{A1})$$

The  $g$  and  $D$  tensors contain information about the orientation of the triplet species as well as about its spatial wave functions. The Hamiltonian is often written in the simplified form A2,

$$H = \beta H \cdot g \cdot S + D(S_z^2 - S^2/3) + E(S_x^2 - S_y^2) \quad (\text{A2})$$

where instead of the five independent elements of the symmetric, traceless  $D$ , only the two scalar zero-field splitting parameters,  $D$  and  $E$ , appear explicitly.<sup>16c</sup> Here the three items of orientational information are implicit in the choice of an axis system which allows the Hamiltonian to be written as (A2).

The standard experimental procedure for determining accurate values of the zero-field parameters has been to locate the principal axis system of  $D$  in preliminary experiments and then to refine  $D$  and  $E$  on the basis of measurements made with the magnetic field along the principal axes.<sup>69</sup> This procedure has a number of practical disadvantages. (1) It requires that the crystal be mounted in special orientations, which are not usually known a priori, thus necessitating several experiments unless a special goniometer is available. (2) It requires that the principal axes of  $g$  and  $D$  be coincident to simplify the secular equation. (3) The principal axes of the tensors are determined separately from the principal values, on different data, and often by analogue techniques.<sup>69b</sup>

Observations made with the laboratory field far from the principal axes are most sensitive to the tensor orientation, and those near the axes are most sensitive to the principal values. But both types of observation contain both types of information and, in the standard approach, much of this information is forfeit. Lin has recently derived a formula by second-order perturbation for using all observations in tensor determination.<sup>70</sup> We have used a different approach involving exact solution of (A1).

With the electron Zeeman eigenstates,  $T_{+1}$ ,  $T_0$ , and  $T_{-1}$ , as a basis set, the matrix of Hamiltonian (A1) is:

where  $z$  is the direction of the applied magnetic field. For a given crystal orientation, the various tensor elements are easily derived from those in a crystal-fixed coordinate system ( $D_{ij}^c$ ) by an appropriate rotation, as for example, (A4)

$$D_{zz} = \sum_{i,j} l_i l_j D_{ij}^c \quad (\text{A4})$$

where the  $l$  are direction cosines between the magnet and crystal coordinate systems.

To first-order  $D$  and  $g$  in crystal coordinates may be found by linear regression from a number of observations of resonance fields for crystals in different general orientations.<sup>16a</sup> Thus the five independent  $D_{ij}^c$  of (A4) may be adjusted for optimum agreement between  $3D_{zz}$  and the observed fine-structure splittings, and the six independent  $g_{ij}^c$  for agreement of  $h\nu/g_{zz}\beta$  with the average of the two resonant fields. Such a treatment can be quite good for fitting the fine structure, but it is usually inadequate for the  $g$  shift.

These first-order tensors may easily be adjusted to yield the correct best-fit tensors by the following iterative procedure.

(1) The first-order tensors are used as a basis for evaluating matrix A3 at the observed fields for resonance in each of the crystal orientations.

(2) These matrices are diagonalized to give exact transition energies for these approximate tensors. This permits estimation of the field at which resonance would be expected.

(3) For each orientation, the difference between observed and expected fine-structure splitting is noted, as is the difference between observed and expected  $g$  shift.

(4) New tensors,  $D'$  and  $g'$ , are fit by least-squares to

these differences in the same way that  $D$  and  $g$  were fit to the original observations.

(5) The approximate  $D$  and  $g$  are corrected by adding  $D'$  and  $g'$ , and the cycle is repeated from 1 until  $D'$  and  $g'$  are zero.

In the case of the methyl-benzoyloxy radical pair, self-consistency was reached for observations in 80 general orientations after a single correction to the first-order tensors. Using the first-order tensors for exact calculation of the transition energies, the rms discrepancy between observed and expected fine-structure splitting was 3.39 G (0.6% of the total range of splittings), and the corresponding discrepancy in  $g$  shift was 3.07 G (20% of the total range). Using the once-corrected tensors, the discrepancies were 3.24 and 0.62 G, respectively. Not surprisingly  $D$  was essentially correct in first order, while  $g$  required significant adjustment to achieve the best least-squares fit.

Given the best tensors in the crystal coordinate system, it is trivial to find both the best orientation of the diagonal tensor and its best principal values. We have also found this procedure to work satisfactorily for triplets with large zero-field splitting.

**Acknowledgments.** We are grateful to the following individuals for helping us with this project: Professors R. B. Davidson, W. C. Danen, M. Fixman, R. L. Fulton, W. B. Hammond, Jr., J. C. Martin, J. Michl, J. S. Vincent, and K. B. Wiberg, Drs. J. Bargon and M. D. Newton, and Mr. J. J. Wendoloski. The X-ray and EPR instruments were purchased with the help of departmental instrument grants from the National Science Foundation. This work was supported by Research Grants GP-14607 and HO-34312 from the National Science Foundation.

**Supplementary Material Available.** Tables VII-X will appear following these pages in the microfilm edition of this volume of the journal. Photocopies of the supplementary material from this paper only or microfiche (105 × 148 mm, 24× reduction, negatives) containing all of the supplementary material for the papers in this issue may be obtained from the Business Office, Books and Journals Division, American Chemical Society, 1155 16th St., N.W., Washington, D.C. 20036. Remit check or money order for \$4.50 for photocopy or \$2.50 for microfiche, referring to code number JACS-75-6729.

## References and Notes

- (1) Taken in part from the Ph.D. dissertation of N. J. Karch, Yale University, 1973, and from the Sixth Form Research Report of E. T. Koh, Hopkins Grammar School, 1970. (b) For a preliminary communication of a part of this work, see N. J. Karch and J. M. McBride, *J. Am. Chem. Soc.*, **94**, 5092 (1972). (c) National Institutes of Health Predoctoral Fellow, 1968–1971; (d) Alfred P. Sloan Research Fellow 1971–1973; recipient of a Camille and Henry Dreyfus Teacher-Scholar Grant.
- (2) For recent reviews, see (a) I. C. Paul and D. Y. Curtin, *Acc. Chem. Res.*, **6**, 217 (1973); (b) M. D. Cohen and B. S. Green, *Chem. Br.*, **9**, 490 (1973).
- (3) For references to the pioneering use of these techniques in studying carbene reactions by Hutchison, Closs, and their collaborators, see C. A. Hutchison, Jr., *Pure Appl. Chem.*, **27**, 327 (1971).
- (4) B. L. Whitsel, R. P. Pankratz, and J. M. McBride, paper in preparation.
- (5) C. Walling and Z. Cekovic, *J. Am. Chem. Soc.*, **89**, 6681 (1967).
- (6) At the higher temperatures, conversion must be kept low to prevent iliquifaction of the sample.
- (7) This analysis assumes that normal and perdeuterated ABP molecules are statistically distributed in the mixed crystals.<sup>9</sup> Differential scanning calorimetry showed no unusual behavior for these crystals.
- (8) A. B. Jaffe, K. J. Skinner, and J. M. McBride, *J. Am. Chem. Soc.*, **94**, 8510 (1972).
- (9) (a) F. D. Greene, H. P. Stein, C.-C. Chu, and F. M. Vane, *J. Am. Chem. Soc.*, **86**, 2080 (1964); (b) C. Walling, H. P. Waits, J. Mlovanovic, and C. G. Pappiaonnou, *ibid.*, **92**, 4927 (1970).
- (10) J. E. Leffler and A. A. More, *J. Am. Chem. Soc.*, **94**, 2483 (1972).
- (11) For details of data analysis including small corrections for incomplete labeling and scrambling in ABP, see N. J. Karch, Ph.D. dissertation, Yale University, 1973.
- (12) R. H. Shapiro and K. B. Tomer, *Org. Mass Spectrom.*, **2**, 1175 (1969).
- (13) We did not check for scrambling in the peroxide during solution photolysis.
- (14) (a) M. Sax and R. K. McMullan, *Acta Crystallogr.*, **22**, 281 (1967); (b) S. Caticha-Ellis and S. C. Abrahams, *Acta Crystallogr., Sect. B*, **24**, 277 (1968); (c) J. Z. Gougoutas and J. C. Clardy, *ibid.*, **26**, 1999 (1970).
- (15) Dr. R. S. Miller in this laboratory has found a peroxide dihedral angle of 143.6° in di-*tert*-butyl diperoxyoxalate (space group *Pbcn*), to be published.
- (16) See, for example, (a) H. C. Box, E. E. Budzinski, and H. G. Freund, *J. Am. Chem. Soc.*, **92**, 5305 (1970); (b) J. E. Wertz and J. R. Bolton, "Electron Spin Resonance", McGraw-Hill, New York, N.Y., 1972, Chapter 10; (c) S. P. McGlynn, T. Azumi, and M. Kinoshita, "Molecular Spectroscopy of the Triplet State", Prentice-Hall, Englewood Cliffs, N.J., 1969, Chapters 9 and 10; (d) L. Salem and C. Rowland, *Angew. Chem., Int. Ed. Engl.*, **11**, 92 (1972); (e) S. H. Glarum in "Chemically Induced Magnetic Polarization", A. R. Lepley and G. L. Closs, Ed., Wiley, New York, N.Y., 1973.
- (17) Since we are concerned with the total difference in energy, influences of opposite sign will cancel.
- (18) When the laboratory field is large and in the direction  $z$ , this interaction varies with crystal orientation and contributes an energy of  $\frac{1}{2}D_{zz}$  (discussed below). The corresponding interaction in  $T_{+1}$  and  $T_{-1}$  contributes an energy of  $-\frac{1}{2}D_{zz}$ .
- (19) A. V. Zubkov, A. T. Koritskii, and Ya. S. Lebedev, *Dokl. Akad. Nauk SSSR*, **180**, 1150 (1968).
- (20) T. Koenig and J. A. Hoobler, *Tetrahedron Lett.*, 1803 (1972).
- (21) We have not yet studied the anisotropy of the  $g$  and hyperfine tensors for the M-P pair in detail. Our preliminary measurements are fully consistent with the nearly isotropic tensors of a phenyl radical<sup>22</sup> and of a spinning methyl radical.
- (22) P. H. Kasal, E. Hedaya, and E. B. Whipple, *J. Am. Chem. Soc.*, **91**, 4364 (1969).
- (23) Photolytic decarboxylation of benzoyloxy radical has been suggested previously, for example, in ref 16a.
- (24) In view of the consistently high isotropic  $g$  factors of the varied acyloxy radicals of Table IV, the value of 2.0058 derived for acetoxy from CIDNP data<sup>25</sup> seems low.
- (25) R. Kaptein, J. Brokken-Zijp, and F. J. J. de Kanter, *J. Am. Chem. Soc.*, **94**, 6280 (1972).
- (26) It has been reported that pairs of benzoyloxy radicals may be observed at low temperature in single crystals of dibenzoyl disulfide doped with benzoyl peroxide and subjected to ionizing radiation.<sup>16a</sup>
- (27) J. A. Pople, D. L. Beveridge, and P. A. Dobosh, *J. Chem. Phys.*, **47**, 2926 (1967).
- (28) For some references, see (a) E. M. Evleth, P. M. Horowitz, and T. S. Lee, *J. Am. Chem. Soc.*, **95**, 7948 (1973); (b) T. Koenig et al., *ibid.*, **96**, 4573 (1974).
- (29) See footnotes *b* and *c* of Table IV.
- (30) See, for example, R. G. Pearson, *Acc. Chem. Res.*, **4**, 152 (1971).
- (31) We are grateful to Professor Josef Michl, University of Utah, for pointing this out to us.
- (32) One might have predicted  $C_{2v}$  geometry for the  $\sigma$  state of  $\text{HCO}_2^+$ , because the  $\sigma^2 A_1$  ground state of isoelectronic  $\text{NO}_2^+$  has  $C_{2v}$  symmetry.<sup>33</sup> This is especially so because qualitatively one would expect a larger splitting between the  $4a_1$  and  $3b_2$  orbitals in  $\text{HCO}_2^+$  than in  $\text{NO}_2^+$ . In  $\text{NO}_2^+$ , the  $2^2 B_2$  state is calculated to lie 3.35 eV above the ground state.<sup>34</sup>
- (33) G. R. Bird et al., *J. Chem. Phys.*, **40**, 3378 (1964).
- (34) R. A. Gangi and L. Burnelle, *J. Chem. Phys.*, **55**, 843 (1971).
- (35) T. Koenig, R. A. Wielesek, and J. G. Huntington, *Tetrahedron Lett.*, 2283 (1974).
- (36) Out-of-plane distortion raised the energy of the optimized  $C_{2v}$   $\pi$  configuration. We did not study out-of-plane distortion from the  $C_s$   $\sigma$  geometry.
- (37) M. D. Newton, personal communication. We are indebted to Dr. Newton for his interest in this problem and for communicating his preliminary results.
- (38) C. P. Slichter, "Principles of Magnetic Resonance", Harper & Row, New York, N.Y., 1963, Chapter 7.
- (39) The assignment of the ground state of the succinyloxy radical as  $^2 A_1$  is almost certainly incorrect. See footnote *c* of Table IV.
- (40) (a) E. Lippmaa, T. Pehk, A. L. Buchachenko, and S. V. Rykov, *Chem. Phys. Lett.*, **5**, 521 (1970); (b) E. M. Schulman, R. D. Bertrand, D. M. Grant, A. R. Lepley, and C. Walling, *J. Am. Chem. Soc.*, **94**, 5972 (1972); (c) A. V. Kessenikh, P. V. Petrovskii, and S. V. Rykov, *Org. Magn. Reson.*, **5**, 227 (1973); (d) J. Bargon, personal communication; (e) B. L. Whitsel, unpublished work in this laboratory.
- (41) This follows directly from equations given by R. Kaptein in ref 16e, pp 140–143. The proportionality constant is of opposite sign for the two radicals.
- (42) Some have claimed a very weak enhanced absorption.
- (43) Our argument is strengthened by considering the effect of nuclear relaxation times on the observed polarization. See C. Walling and A. R. Lepley, *J. Am. Chem. Soc.*, **94**, 2007 (1972).
- (44) On the basis of unpublished experiments and INDO calculations, Bargon believes that the ground state of benzoyloxy radical in solution is a  $\pi$  state with the carboxyl and phenyl groups in perpendicular planes. The  $D$  tensor we observe shows that, in irradiated crystalline ABP, the radical is nearly planar. This planarity could result from matrix constraints since Bargon calculates a small energy difference between the perpendicular and the planar geometries.<sup>40c</sup>
- (45) The splitting is defined as the field at which the  $T_{-1} \rightarrow T_0$  transition is observed minus the field at which  $T_0 \rightarrow T_1$  is observed at constant microwave frequency. The simple relationship with  $D_{zz}$  holds only to first order. We have solved for the exact least-squares  $D$  tensor by an iterative procedure, but this tensor is within experimental error of the first-order tensor (see Table VI). Our energy units for  $D$  are gauss which may be converted to other units through multiplication by  $g\mu_B\beta$  (2.8025 MHz/G or  $9.348 \times 10^{-5}$  cm<sup>-1</sup>/G).
- (46) No directional information is available from powdered or glassy sam-

- ples, and only two values are reported: *D*, one half the absolute value of the largest fine-structure splitting; and *E*, one sixth the range of splittings in the perpendicular plane.
- (47) This may reflect inadequacy of first-order perturbation theory since exact refinement of another data set gave somewhat greater improvement using a traceless tensor. See entry 11a of Table VI.
- (48) R. McWeeny, *J. Chem. Phys.*, **34**, 399 (1961).
- (49) That the benzoyloxy oxygens of the starting material lie in this plane argues strongly against a perpendicular geometry for the benzoyloxy radical we are observing.<sup>44</sup>
- (50) H. A. Scheraga, *Adv. Phys. Org. Chem.*, **6**, 103 (1968), Table 16.
- (51) Hydrogens of the methyl radical were omitted.
- (52) It is possible that, in the solid state, acetoxy and benzoyloxy radicals recombine efficiently without oxygen scrambling.<sup>53</sup> M-B might then be formed only in rare instances when peroxide homolysis and decarboxylation are concerted.
- (53) For an analogous difficulty in solution thermolysis, see J. C. Martin and J. H. Hargis, *J. Am. Chem. Soc.*, **91**, 5399 (1969).
- (54) K. J. Skinner, R. J. Blaskiewicz, and J. M. McBride, *Isr. J. Chem.*, **10**, 457 (1972).
- (55) C. Walling and E. A. McElhill, *J. Am. Chem. Soc.*, **73**, 2927 (1951); cf. Yu. A. Ol'dekop, A. N. Sevchenko, I. P. Zyat'kov, G. S. Bylina, and A. P. El'nitskii, *Dokl. Akad. Nauk SSSR*, **128**, 1201 (1959).
- (56) V. R. Kokatnur and M. Jelling, *J. Am. Chem. Soc.*, **63**, 1432 (1941).
- (57) L. Syper, *Tetrahedron Lett.*, 4493 (1966).
- (58) A. Murray, III, and D. L. Williams, Ed., "Organic Synthesis with Isotopes", Part II, Interscience, New York, N.Y., 1958; A. I. Vogel, "Textbook of Practical Organic Chemistry", 3rd ed, Wiley, New York, N.Y., p 367.
- (59) J. C. Martin and S. A. Dombchik, *Adv. Chem. Ser.*, **75**, 269 (1968).
- (60) We are grateful to Professor Martin for communicating this method for increased O<sub>2</sub> recovery prior to publication.
- (61) D. S. Tarbell and E. J. Longosz, *J. Org. Chem.*, **24**, 774 (1959).
- (62) See W. R. Busing et al., Report ORNL-4143, Oak Ridge National Laboratory, Oak Ridge, Tenn., 1968.
- (63) The mean calculated *F* for these reflections in the final refinement cycle was 1.17.
- (64) G. H. Stout and L. H. Jensen, "X-Ray Structure Determination", Macmillan, New York, N.Y., 1968, p 457.
- (65) We thank Professor M. Saunders for a listing of the original program.
- (66) W. R. Busing, K. O. Martin, and H. A. Levy, "OR XFLS3", Oak Ridge National Laboratory, Oak Ridge, Tenn., 1971. Minimizing  $\sum w(|F_d| - |F_c|)^2$ . Scattering factors for hydrogen were taken from R. F. Stewart, E. R. Davidson, and W. T. Simpson, *J. Chem. Phys.*, **42**, 3175 (1965); for carbon and oxygen from D. T. Cromer and J. B. Mann, *Acta Crystallogr., Sect. A*, **24**, 321 (1968).
- (67) Manufacturer's specifications.
- (68) Reference 16b, p 465.
- (69) (a) C. A. Hutchison, Jr., and B. W. Mangum, *J. Chem. Phys.*, **34**, 908 (1961); (b) O. Rohde, S. P. Van, W. R. Kester, and O. H. Griffith, *J. Am. Chem. Soc.*, **96**, 5311 (1974).
- (70) W. C. Lin, *Mol. Phys.*, **25**, 247 (1973).

## Lone Pair-Polar Bond Hyperconjugation in Carbon-Halogen Chemistry

Richard C. Bingham

Contribution from the Organic Chemicals Department, E. I. Du Pont de Nemours and Company, Jackson Laboratory, Wilmington, Delaware 19898.

Received February 18, 1975

**Abstract:** Molecular orbital theory suggests that the importance of vicinal lone pair-polar bond hyperconjugation (e.g.,  $XCH_2-CH_2^- \leftrightarrow X-CH_2=CH_2$ ) should increase, when X represents halogen, in the order  $F < Cl < Br < I$ . This pattern, which is determined by the carbon-halogen bond strengths, contrasts with that predicted by the valence bond description of this phenomenon. A variety of available experimental data, including the conformational equilibria of 2-halotetrahydropyrans (the anomeric effect), 2-halocyclohexanones and allyl halides, the rotational barriers of *N,N*-dimethylcarbonyl halides, and the acidities of haloacetic acids, support the molecular orbital interpretation. These results serve to demonstrate that anionic hyperconjugation is, indeed, a very real, general, and important concept.

The possible importance of lone pair-polar bond hyperconjugation in organic fluorine chemistry was first suggested in 1950.<sup>1</sup> The subject remains controversial to this date, primarily because the effects typically attributed to such hyperconjugation are generally small and therefore difficult to interpret unambiguously for the isolated fluorine case.<sup>2</sup>

Lone pair-polar bond hyperconjugation is described in valence bond terminology by the resonance hybrids **1** and **2**.



In this view, hybrid **2** should be stabilized by electronegative X. The importance of hyperconjugation should increase correspondingly. Fluorine, by virtue of its high electronegativity, is therefore expected to be more disposed to hyperconjugate with vicinal lone pairs than other substituents.<sup>3</sup> More sophisticated analyses of this subject based on simple perturbation theory advocate the same conclusion.<sup>4</sup> We submit, on the contrary, that the following discussion strongly indicates that, in the halogen series, the importance of lone pair-polar bond hyperconjugation actually increases in the order  $C-F < C-Cl < C-Br < C-I$ . Recognition of this trend provides a new basis upon which to judge the general significance of hyperconjugation of this type.

Lone pair-polar bond hyperconjugation is best described as a stabilizing, internal charge transfer between the doubly occupied lone pair orbital (*n*) and the unoccupied  $\sigma^*$  orbital of the vicinal polar bond (Figure 1a).<sup>4</sup> The magnitude of this interaction, and hence the degree of stabilization derived therefrom, increases as the energy separation ( $\Delta E$ ) between the orbitals decreases.<sup>4,5</sup>

In the molecular orbital theory of bonding, the energy separation between the  $\sigma$  and  $\sigma^*$  (or  $\pi$  and  $\pi^*$ ) orbitals of a chemical bond increases with increasing bond strength. Carbon-halogen bond strengths decrease in the order  $C-F > C-Cl > C-Br > C-I$  (see Table I).<sup>6</sup> The  $\sigma-\sigma^*$  splitting of these bonds should decrease proportionally. Assuming a symmetrical displacement of  $\sigma$  and  $\sigma^*$  orbitals below and above, respectively, an arbitrary nonbonding level, the energy of the  $\sigma^*$  orbitals of carbon-halogen bonds should increase in the order  $I < Br < Cl < F$  as illustrated in Figure 1b.

Both the  $\sigma$  and  $\sigma^*$  orbitals of a C-X bond are expected to be lowered in energy as the electronegativity of X increases.<sup>4</sup> While this shift should be largest for fluorine, it is not unreasonable to expect that the overall trend in orbital energies will remain as predicted by the relative bond strengths. Two sets of experimental data provide support